EPJ Web of Conferences **102**, 00012 (2015)
DOI: 10.1051/epjconf/201510200012


# Disk Chemistry*

Wing-Fai Thi

[1] *MPE, Garching, Germany*

**Abstract.** The chemical species in protoplanetary disks react with each other. The chemical species control part of the thermal balance in those disks. How the chemistry proceeds in the varied conditions encountered in disks relies on detailed microscopic understanding of the reactions through experiments or theoretical studies. This chapter strives to summarize and explain in simple terms the different types of chemical reactions that can lead to complex species. The first part of the chapter deals with gas-phase chemistry and the second part introduces chemical reactions occurring on grain surfaces. Several terms pertaining to astrochemistry are introduced.

## 1 The role of chemistry in disk and planet-formation processes

Chemistry are not only processes that trace the physical conditions in disks but they also plays important roles in controlling the dynamics of disks or aspects of planet formation and provide the primordial composition of planets.

The most promising explanation to drive mass accretion in disks and explain the disk evolution is turbulence driven by magneto-rotational instability because molecular viscosity is inefficient on large scales. Magneto-rotational instability is a ideal-MHD phenomenon that occurs only if the gas is sufficiently ionized to couple dynamically to the magnetic fields. The strength of gas turbulence is characterized by the factor $\alpha$ so that the large scale turbulence can be written as $\nu = \alpha c_s h$ (with $c_s$ the sound speed and $h$ the gas scale height of the disk). Many non-ideal MHD resistivities can restrict the development of MRI turbulence. The resistivities (Ohmic and Ambipolar diffusion) depend on the abundances of the charge carriers among other factors. Therefore the detailed knowledge of the disk ionization state is central to understand disk dynamical evolution.

In planet formation, chemistry defines the disk region where water can be frozen onto grains, the so-called ice zone where grains can coagulate more easily. The ice zone is paramount to permit the formation of giant planets via the core-accretion model. The unusual C/O abundance ratios seen in exoplanets raise the question of chemical filtering in disks (Helling et al. 2014; Öberg et al. 2011).

## 2 The path to complexity

Chemistry is also central to questions related to the origin of life. One major question is whether complex organic molecules (COMs) were originally produced in the young Earth and/or had an extra-terrestrial origin. The original composition of Earth's atmosphere (and of terrestrial extrasolar planets)

*11th Lecture of the Summer School "Protoplanetary Disks: Theory and Modelling Meet Observations"

influenced the conditions for the emergence of life but remains a major subject of debate (Chyba & Sagan 1992; Ehrenfreund & Charnley 2000) . The molecules in the primordial atmosphere and oceans are the building blocks for the prebiotic molecules. It is believed that a combination of comets and other extraterrestrial bodies such as meteorites and interplanetary dust particles may have supplied the primordial soup with extraterrestrial complex organic molecules.

In the following sections, we will detail few ideas needed to understand the different types of chemical reactions that can occur in protoplanetary disks. Many good textbooks deal with the chemistry in the interstellar medium and we refer the reader to those references (Dyson & Williams 1997; Lequeux 2005; Tielens 2010).

## 3 Chemical reactions

A chemical reaction can be split into steps: the collision between the reactants, the destruction of existing chemical bonds followed by the formation of new bonds, and the removal of the excess energy for exothermic reactions. The first and last steps limit the efficiency of chemical reactions in the low density space environments. In the following sections, those steps will be discussed in details.

### 3.1 Collision frequency and chemical equilibrium

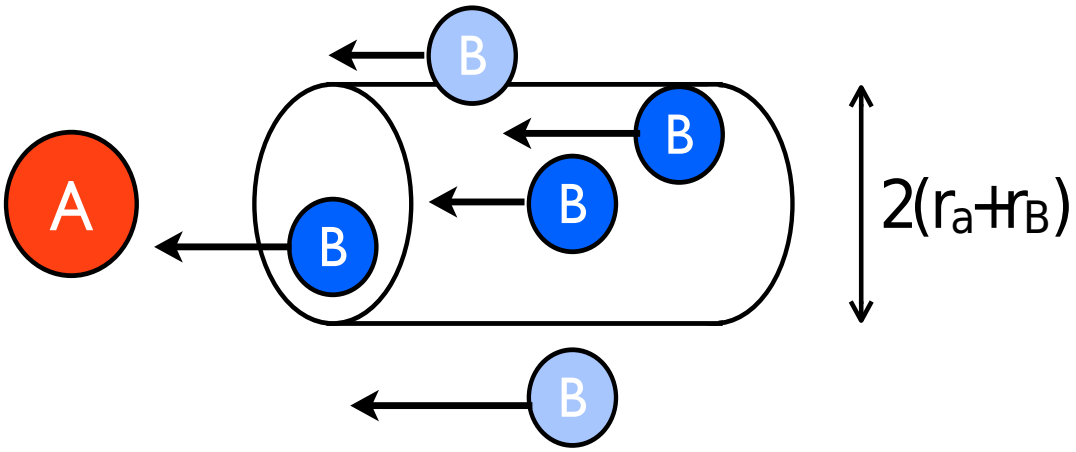


**Figure 1.** Hard sphere collisions.

Like all physical phenomena, any chemical reaction needs to conserve the energy and the angular momentum. The simplest possible description of a chemical reaction is the so-called "hard-sphere" or "billiard ball" approximation where a species is considered as a perfect sphere with a constant radius $r$ (Fig. 1). Another simplification is that there is no short- or long-range electromagnetic interaction, which can decrease or enhance significantly the reaction rates. The "hard-sphere" collisional frequency between two species A and B within a unit volume each second is given by

$$z_{\rm AB} = \langle \sigma_{\rm AB} v \rangle \, n_{\rm A} n_{\rm B} = \sigma_{\rm AB} \left( \frac{8kT}{\pi \mu_{\rm AB}} \right)^{1/2} n_{\rm A} n_{\rm B}, \tag{1}$$

where $\sigma_{\rm AB} = \pi(r_{\rm A} + r_{\rm B})^2$ is the collisional cross-section with $r_{\rm A}$ and $r_{\rm B}$ the Van der Waals radii, $\mu_{\rm AB} = m_{\rm A} m_{\rm B}/(m_{\rm A} + m_{\rm B})$ is the reduced mass, $n_{\rm A}$ and $n_{\rm B}$ the number density of species A and B. Here,

$T$ is the gas temperature and $k$ the Boltzmann constant. The typical radius of an atom is $\sim 1.5\times10^{-8}$ cm (1.5 Å), giving a cross-section of $\sim 3\times10^{-15}$ cm$^2$. The reduced mass is $\sim 1\times10^{-24}$ g. At 10 K, the mean velocity assuming a Maxwellian distribution is $\sim$60 000 cm s$^{-1}$. An abundant species has an abundance of $10^{-6}$–$3\times10^{-4}$ compared to hydrogen nuclei. This results from the elemental abundance of the constituents. Thus for a gas number density of $n_{\rm H}$ of $10^6$ cm$^{-3}$, $n_{\rm A} \simeq n_{\rm B} \sim 1-100$ cm$^{-3}$. The maximum collisional frequency between two abundant species is $1.5\times10^{-6}$ s$^{-1}$ or $\sim 0.8$ days. For a density of $10^{12}$ cm$^{-3}$, the frequency is increased by a factor $10^{12}$. Interestingly, if no reaction proceeds upon the encounter, the collision is elastic and its collision cross section has the same order of magnitude as collision de-excitation rates by molecular hydrogen ($\sim 10^{-10}$ cm$^3$ s$^{-1}$).

For three-body collisions, the frequency is much less amenable to a simple understanding. The hard sphere radius is given by the symmetric formula $r_0 = (r_{\rm AB} r_{\rm BC} r_{\rm CA})^{1/3}$, and the cross-section in the 6-dimensional hypersphere is $\sigma_{\rm ABC} = (8\pi^2/15) r_0^5$. The collisional frequency is

$$z_{\rm ABC} = \sigma_{\rm ABC} \frac{15\pi}{8} \left( \frac{kT}{2\pi\mu_{\rm ABC}} \right)^{1/2} n_{\rm A} n_{\rm B} n_{\rm C}, \tag{2}$$

where the three-body reduced-mass is

$$\mu_{\rm ABC} = \left( \frac{m_{\rm A} m_{\rm B} m_{\rm C}}{m_{\rm A} + m_{\rm B} + m_{\rm C}} \right)^{1/2} \tag{3}$$

Let us consider the three-body reaction $H_2$ + CH + M $\rightarrow$ $CH_3$ + M, where the collision partner M is $H_2$. The different values are: $r_{\rm AB} = r_{\rm BC} \simeq 9.2 \times 10^{-9}$ cm, $r_{\rm CA} \simeq 5.7 \times 10^{-9}$ cm, $m_{\rm A} = 2$ amu, $m_{\rm B} = 13$ amu, and $m_{\rm C} = 2$ amu, where the atomic mass unit amu = $1.66 \times 10^{-24}$ g. For a hydrogen density of $10^6$ cm$^{-3}$, with hydrogen being fully molecular, and a CH abundance of $10^{-6}$, the collisional frequency is $\sim 2 \times 10^{-24}$ s$^{-1}$. At $10^{12}$ cm$^{-3}$ the frequency is increased by a factor $(10^6)^3 = 10^{18}$. Therefore except for the very dense inner disk region, most reactions occurring in protoplanetary disks will involve one or two species. Chemical reactions occur at the same time than other processes such as dynamics and diffusion or elastic collisions. The different chemical timescales should be compared to dynamical and heating/cooling timescales.

### 3.2 The "hard collision" approximation

A major shortcomings of the "hard-sphere" theory is that molecules are neither spheres nor symmetric. The orientation of the collisions determine whether a reaction can occur. In addition atoms and molecules interact via long- and short-range electromagnetic interactions. Chemical reactions are theoretically studied by solving conservation equations quantum mechanically. However, many insights can be provided by a classical approximation called the "hard collision" approximation. A hard collision is considered to be a classical collision in which for a given incident relative energy the impact parameter $b$ is small enough such that the particles can surmount the angular moment barrier. The hard collision approximation provides not only valuable insight in the physics of reactive reactions, it gives values that can be close to the actual ones, either computed by quantum theories or measured experimentally. For instance, ion-molecule reactions occur close to the "hard collision" rate and neutral-neutral reactions without activation energy barrier often proceed at every collision.

### 3.3 Chemical bonds and thermochemistry

A typical chemical reaction can be written in the form

$$\rm A + B + M \rightleftharpoons C + D + M + \Delta \mathit{E}, \tag{4}$$

where we assumed that the reaction is exothermic to the right ($\Delta E > 0$), and M is a third body, which is mainly one of the three major species H, $H_2$, or He. For densities below $10^{12}$ cm$^{-3}$, only one-body or two-body reactions occur.

The thermochemistry of a reaction can be evaluated from the enthalpy ($H$) difference between products (C and D) and reactants (A and B)

$$\Delta H(\text{reaction}) = H(\text{products}) - H(\text{reactants}), \tag{5}$$

where a negative enthalpy corresponds to release of energy by a reaction ($\Delta E = -\Delta H$). Enthalpies depend on the temperature, the phase of the species, and the stoichiometry of the reaction. Table 1 summarizes the bond energies, i.e. the energies required to break certain bonds. For a stable species, the heat of formation is generally negative (i.e. the reaction is exothermic).

**Table 1.** Average bond enthalpies (1 KJ/mol = 120 K = 0.01 eV)

| Bond | (KJ/mol) | Bond | (KJ/mol) | Bond | (KJ/mol) |
|---|---|---|---|---|---|
| H-H | 436 | O-H | 463 | C=C | 614 |
| C-H | 413 | O-O | 146 | C≡C | 839 |
| C-C | 348 | S-H | 339 | C=N | 615 |
| C-N | 293 | S-S | 266 | C≡N | 891 |
| C-O | 358 | S=O | 523 | C=O | 799 |
| C-S | 259 | S≡S | 418 | C≡O | 1072 |
| N-H | 391 | | | N=N | 418 |
| N-N | 163 | | | N≡N | 941 |
| N-O | 201 | | | O=O | 495 |

## 4 Formation of bonds

The first category of reactions involves the formation of new bonds between two reactants A and B (A+B $\rightarrow$ AB$^*$ $\rightarrow$ A + B ). The main difficulty with these reactions is to stabilize the newly formed complex (AB$^*$) either thorough the emission of a photon, the collision with a third partner, or the emission of an electron for gas-phase reactions. A complex is a long-lived intermediate molecule with a total internal energy above its dissociation limit. Interestingly, for surface reactions, the surface or the breaking of the adsorption bond to the surface can act as a heat sink. Therefore certain highly exothermic reactions can proceed on grain surfaces but not in a low-density gas.

An association reaction (A$^+$+B $\rightarrow$ AB$^+$, with rate $k_{\rm ass}$) occurs via the formation of an activated complex (excited (AB$^+$)$^*$), which has to be stabilized through the emission of a photon or though collision with a third body. Otherwise the complex will revert back to the initial parent species. The reaction can be decomposed into elementary steps (Klippenstein et al. 1996). The first elementary step is the formation of the complex A+B $\rightarrow$ (AB$^+$)$^*$ with rate $k_f$. The complex can re-dissociate into the initial species ((AB$^+$)$^*$ $\rightarrow$ A$^+$ + B, with rate $k_b$), or can be stabilized by collision with a third body ((AB$^+$)$^*$ + M $\rightarrow$ AB with rate $k_c$). The stabilization can also be achieved by the emission of a photon ((AB$^+$)$^*$ $\rightarrow$ AB$^+$ + h$\nu$, with rate $k_r$). The effective rate is

$$k_{\rm ass} = k_{\rm eff} = \frac{k_f(k_r + k_c n_{\rm M})}{k_b + k_r + k_c n_{\rm M}}. \tag{6}$$

In the low-density regime, the rate can be expanded in a Taylor series

$$k_{\rm eff} \simeq \frac{k_f k_r}{k_b + k_r} + \frac{k_f k_b k_c}{(k_b + k_r)^2} n_{\rm M}. \tag{7}$$

At very low densities, like in most regions in space, the rate simplifies further

$$k_{\rm eff} \simeq \frac{k_f k_r}{k_b + k_r}. \tag{8}$$

In the high-density (i.e. high-pressure) regime, or in the so-called high-efficiency regime when $k_r \gg k_b$, the rate becomes

$$k_{\rm eff} \simeq k_f \tag{9}$$

On the other hand unimolecular redissociation ($AB^* \rightarrow A + B$) occurs much faster than emission of a photon if $k_b \gg k_r$. This is the so-called low-efficiency limit.

$$k_{\rm eff} \simeq k_f \frac{k_r}{k_b}. \tag{10}$$

### 4.1 Radiative association

The high-efficiency regime corresponds to radiative association. The radiative rate $k_r$ can be written within the harmonic approximation as (Klippenstein et al. 1996)

$$k_r(\mathrm{s}^{-1}) = \sum_{i=1}^{N_m} \sum_{n=0}^{\infty} 1.25 \times 10^{-7} n P_i(n)\, I_i(\mathrm{km/mol})\, \nu_i^2(\mathrm{cm}^{-1}), \tag{11}$$

where $N_m$ is the number of vibrational modes, $P_i(n)$ is the probability of vibrational mode $i$ being in level $n$, $I_i$ is the infrared absorption intensity for the $v = 0$ and $v = 1$ transition of mode $i$, and $\nu_i$ is the $i$-th vibrational frequency. The population probability can be approximated by

$$P_i(n, T) = \exp\left(-\frac{h\nu_i n}{kT}\right)\left[1 - \exp\left(-\frac{h\nu_i}{kT}\right)\right]. \tag{12}$$

Since the energy of the excited complex is spread over all available degrees of freedom, the larger the complex, the larger the rates can be. Methanol has for example 12 vibrational modes. The vibrational transition time-scales are of the order of $10^{-3}-10^{-2}$ s, while the reaction collision time-scale is of the order of $10^{-13}$ s. Electronic allowed transitions are faster with a time-scale of the order of $10^{-8}$–$10^{-7}$ s. We are well within the low-efficiency regime and only one complex out of $(k_r/k_b)^{-1} \sim 10^6$ would result in a stable product. In the interstellar medium and in disks, the main reactions of this type involve an ion and a neutral species ($A^+ + B \rightarrow (AB^+)^* \rightarrow AB^+$). A complex formation rate between an ion and a neutral species follows the Langevin encounter rate $k_f \sim 10^{-10}-10^{-9}$ s$^{-1}$, thus association reactions rates would be of the order of $10^{-16}-10^{-17}$ s$^{-1}$.

### 4.2 T(h)ermolecular reactions (3-body reactions)

Three body reactions ($A + B + M \rightarrow AB + M$) have rates of the order of $10^{-32}$ cm$^6$ s$^{-1}$ and are thus efficient for densities higher than $10^{12}$ cm$^{-3}$. The third-body carries the excess energy of the intermediate complex away.

### 4.3 Associative detachment

The reaction between an anion to a neutral species results in a neutral product that is stabilized through the release of an electron ($A + B^- \rightarrow AB + e$). The most important associative detachment reaction is $H + H^- \rightarrow H_2 + e$, with a rate of $1.3{\times}10^{-9}$ cm$^3$s$^{-1}$. In the absence of dust grains in the Early Universe, this reaction is the only way to form molecular hydrogen.

### 4.4 Radiative recombination

Radiative recombinations involve cations and are the inverse reactions of photoionizations $AB^+ + e \rightarrow AB^* \rightarrow AB + h\nu$. Therefore radiative recombination rates can be estimated by detailed balance between the two processes

$$n(e)n(X_i)\alpha_T = n(X_0)\int_0^\infty \sigma(\nu)B(\nu)d\nu, \tag{13}$$

where $B(\nu)$ is the blackbody photon flux. The ?namical equilibrium is given by the Saha equation. Since a typical value for the photoionization cross-section is $\simeq 10^{-17}$ cm$^2$, the rate coefficients for radiative recombinations are $\simeq 10^{-12}$ cm$^3$ s$^{-1}$.

The lack of efficient relaxation processes or the need to create first an anion makes the direct formation of new bonds very slow in general except for special circumstances (i.e. high gas densities).

## 5 Rearrangement of bonds

Reaction between two species A and B can result in exchanging part of each species to form species C and D. For these reactions the excess energy is mostly converted into kinetic energy for the products. In general, bond rearrangements favor the most strongly bound pair of atoms.

### 5.1 Ion-neutral reactions

The first type of rearrangement reactions involve one charged species and a neutral partner. Reactions between an ion $A^+$ and a neutral species B ($A^+ + B \rightarrow C^+ + D$) occur rapidly because the strong long-range polarization-induced interaction potential (charge/quadrupole-induced interaction $\propto 1/r^4$) can be used to overcome any activation barrier involved. The long range potential is

$$V(r) = -\frac{\alpha e^2}{2r^4}, \tag{14}$$

where $\alpha$ is the polarizability of neutral species($\sim 10^{-24}$ cm$^3$), $e$ the electron charge, and $r$ the distance from the nucleus. The total energy of the system is

$$E = \frac{1}{2}\mu_{AB}r^2 + E\frac{b^2}{r^2} + V(r), \tag{15}$$

where $\mu_{AB}$ is the reduced mass and $b$ the impact parameter. The maximum impact parameter $b_m$ for which the particles will spiral inward is a value just smaller than the impact parameter that leads to orbiting one around one another (Fig. 2). The orbiting requirement is that at the radius of closest approach $r_c$, the effective potential is flat. Thus

$$\frac{1}{2}\mu_{AB}v_\infty^2 = \frac{1}{2}\mu v_\infty^2\frac{b_m^2}{r_c^2} + V(r_c) \tag{16}$$

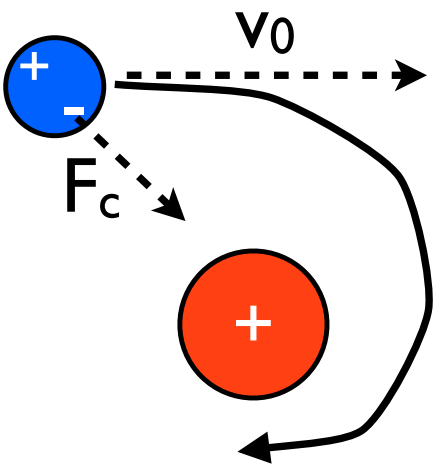


**Figure 2.** Capture theory.

and

$$0 = -\mu_{\rm AB} v_\infty^2 \frac{b_{\rm m}^2}{r_{\rm c}^3} + \left.\frac{\partial V(r)}{\partial r}\right|_{r_{\rm c}}, \tag{17}$$

with $v_\infty$ the velocity at infinity ($v_\infty = \sqrt{8kT/\pi\mu_{\rm AB}}$). The result is

$$b_{\rm m} = \left(\frac{2}{v_\infty}\right)^{1/2} \left(\frac{\alpha e^2}{\mu_{\rm AB}}\right)^{1/4} \tag{18}$$

The "hard"-collision (Langevin) rate coefficient is

$$k_{\rm L} = \langle \sigma v \rangle = \int \pi b_{\rm m}^2 v f(v) dv = 2\pi \left(\frac{\alpha e^2}{\mu_{\rm AB}}\right)^{1/2}, \tag{19}$$

where $f(v)$ the Maxwellian velocity distribution. $k_{\rm L}$ is of the order of $10^{-9}$ s$^{-1}$ and is not temperature-sensitive. If the neutral species has a permanent dipole moment $\mu_{\rm D}$, the enhanced rate is given by the average dipole orientation theory (Bass et al. 1975)

$$k_{\rm dip} = 2\pi \left( \left(\frac{\alpha}{\mu_{\rm AB}}\right)^{1/2} + \mu_{\rm D} \left(\frac{2}{\pi \mu_{\rm AB} kT}\right)^{1/2} \right). \tag{20}$$

The enhancement is particularly strong at low temperatures. At low temperatures, the ion-neutral reactions, combined with the dissociation recombination reactions are the most efficient to form simple molecules. Ion-neutral reactions are driven by ionization (by cosmic-rays, X-rays, or radioactive decay).

### 5.2 Kinetic rate temperature-dependence as function o the shape of the long-range interaction

Ion-neutral reactions are only one type of reactions where long-range interactions control the temperature-dependance of the rates. The adiabatic capture centrifugal sudden approximation provides estimates of the temperature-dependance of the rate coefficients on the shape of the long-range

attractive intermolecular interaction potential

$$k(T) \propto T^{-\frac{2}{n}+\frac{1}{2}}, \tag{21}$$

for a potential of the form $r^{-n}$ when $T \to 0$. Table 2 lists a number of interactions with their temperature dependence at low temperatures. Ion-neutral reactions are the fastest reactions at low temperatures. Since one of the products is also a cation, further ion-neutral reactions can proceed rapidly leading to molecular cations that can in turn recombine with an electron.

**Table 2.** Temperature-dependance of the rate coefficients at low temperatures.

| Interaction | Potential | $k$ (low T) |
|---|---|---|
| Charge-dipole | $r^{-2}$ | $T^{-1/2}$ |
| Charge-quadrupole | $r^{-3}$ | $T^{-1/6}$ |
| Dipole-dipole | $r^{-3}$ | $T^{-1/6}$ |
| Charge-induced dipole | $r^{-4}$ | $T^{0}$ |
| Dipole-quadrupole | $r^{-4}$ | $T^{0}$ |
| Dispersion | $r^{-6}$ | $T^{-1/6}$ |

### 5.3 Charge-transfer reactions

Charge transfer reactions involving an atom are key to the ionization balance. When a molecule is involved, rates can be as high as $10^{-9}$ cm$^3$ s$^{-1}$ in the exothermic direction if there is an energy level in the product that is resonant (i.e. close within 0.1 eV) with the recombination energy and the Franck-Condon factor connecting the upper and lower states is large. In general molecules have more states available than atoms ($A^+ + B \rightarrow A + B^+$).

### 5.4 Neutral-neutral reactions

A detailed review on recent works on neutral-neutral reactions is given by Smith (2008). The discussion here is kept at an elementary level. The attractive interaction in neutral-neutral reactions is due to van der Waals forces that are efficient at short distances only (the potential is $\propto 1/r^6$). The simplest representation of the interaction between neutral species is the Lennard-Jones potential

$$V(r) = \epsilon \left[ \left( \frac{r_\mathrm{m}}{r} \right)^{12} - 2 \left( \frac{r_\mathrm{m}}{r} \right)^{6} \right], \tag{22}$$

where $r$ is the distance between the particles (Fig. 3). $\epsilon$ is the depth (i.e. the minimum) of the potential well and $r = r_\mathrm{m}$ is the distance at which the minimum is reached. At large distances, the attractive second term in the potential dominates

$$V(r) \simeq -\frac{\alpha_1 \alpha_2}{r^6} I, \tag{23}$$

where $\alpha_1$ and $\alpha_2$ are the polarizabilities of the two particles ($\sim 10^{-24}$ cm$^3$) and $I$ is a characteristic energy related to the ionization energies ($I \sim 1$ Rydberg, or 13.6 eV). The "hard" collision impact parameter for neutral-neutral reactions is

$$b_\mathrm{m}^2 = (3/2)^{2/3} \left( \frac{6 \alpha_1 \alpha_2 I}{\mu_\mathrm{AB} v_\infty} \right)^{1/3}. \tag{24}$$

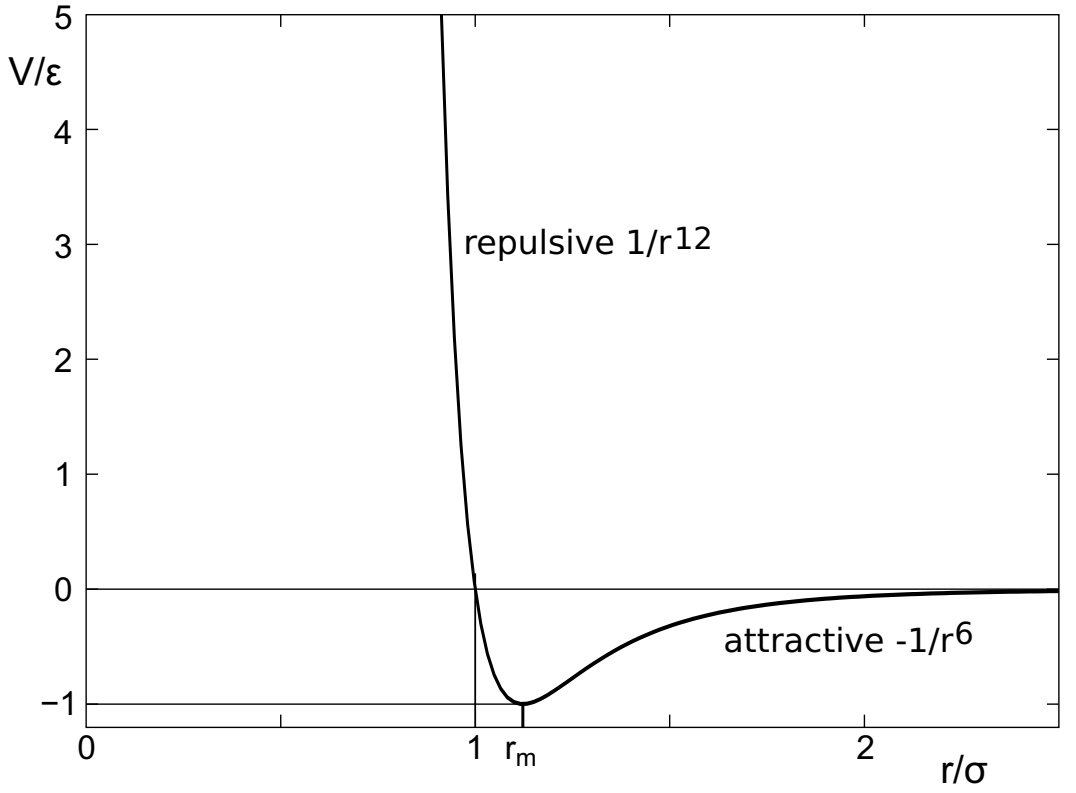


**Figure 3.** Lennard-Jones interaction potential.

The approximate rate coefficient is

$$k_{\rm nn} \simeq \pi (3/2)^{2/3} \left( \frac{6\alpha_1 \alpha_2 I}{\mu_{\rm AB}} \right)^{1/3} \langle v^{1/3} \rangle \simeq 4 \times 10^{-11} (T/100)^{1/6} \ \ {\rm cm}^3 \ {\rm s}^{-1}, \tag{25}$$

with $\mu_{\rm AB} = 2$ amu. Neutral-neutral reactions involving atoms or radicals with an unpaired electron (e.g. OH, CN) have low or no activation barriers. The rate coefficients are in the form

$$k_{\rm nn} = a(T/300)^b = A(T)\,. \tag{26}$$

Many neutral-neutral reactions involve the breaking of chemical bonds before the rearrangement, hence possess an activation barrier $E_a$, which is defined as the difference in energy between the reactant state and the highest energy transition state. The transition state theory has been proposed to calculate reaction rates and in particular provides a way to calculate $E_a$. A reaction with an activation barrier can be exothermic or endothermic and the activation energy does not correlate with the overall energetics of a reaction. Simple considerations can be used to determine if a given reaction will involve the breaking of bonds and therefore an activation barrier exists. Let us take the example of the reaction O + CH. Without a priori knowledge three products are possible: CO, OH, and HCO. In Table 3, we listed the rates for the formation of CO and OH. The reaction leading to CO has no barrier, while the one leading to OH has one ($E_{\rm a} = 2381$ K). A simple reasoning involves the potential

transition state complexes: O...C-H ($\rightarrow$ HCO$^*$ $\rightarrow$ CO + H) and C-H...O ($\rightarrow$ C + OH). CH is a radical. A radical is an atomic or molecular species having an unpaired or odd electron. Some radicals such as nitric oxide (NO) are relatively stable, but most are reactive. CH is the simplest example of a group of molecules called carbyne. Carbyne molecules are generally found to be in electronic doublet states: the nonbonding electrons on carbon are arranged as one radical (unpaired electron) and one electron pair, leaving a vacant atomic orbital, rather than being a triradical (the quartet state). More precisely, the CH radical has an electron configuration $1\sigma^2\ 2\sigma^2\ 3\sigma^2\ 1\pi$ (:$\dot{\text{C}}$-H). The formation of the O...C-H complex does not involve the breaking of a bond (O bonds with the unpaired electron) while the formation of the C-H...O requires the weakening of the strong C-H bond. In general the breaking of the C-H, O-H, or N-H bonds require substantial energies.

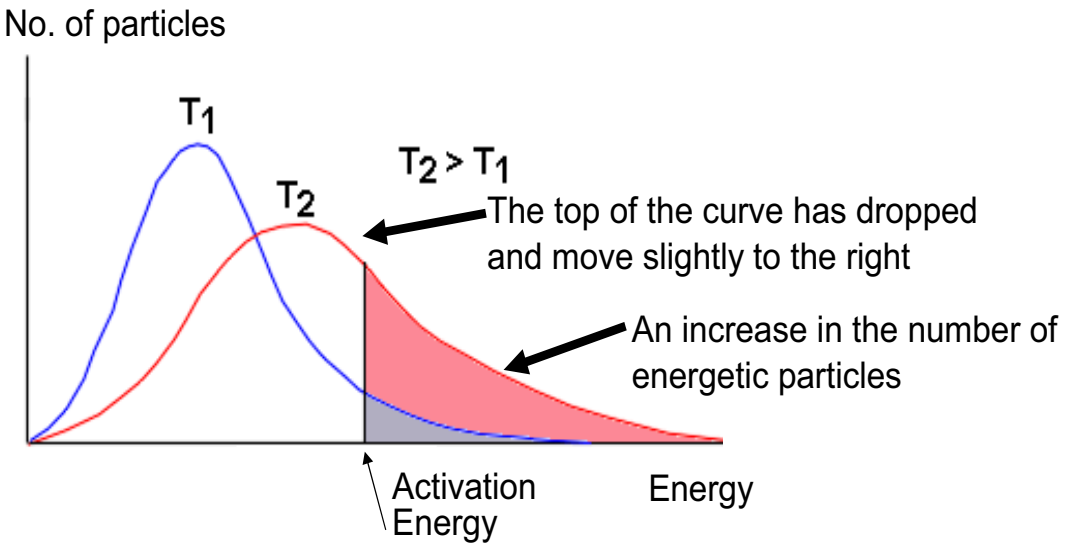


**Figure 4.** Maxwellian energy distribution and activation energy.

The velocity of the gas at temperature $T$ follows a Maxwellian distribution (Fig. 4). The reaction rate for a Maxwellian gas is

$$k_{\rm nn} = \left(\frac{8}{\pi\mu_{\rm AB}(kT)^3}\right)^{1/2} \int_0^\infty S_{\rm AB}\, E\, {\rm e}^{-\frac{E}{kT}}\, dE. \tag{27}$$

The cross-section $S_{\rm AB}$ has to accommodate the activation barrier. The main assumption is that only the kinetic energy directed along the line centers is important. The collisional cross-section is modified to account for the fact that only reaction occurring with relative energy $E = \mu_{\rm AB} v_r^2/2$, where $v_r$ is the

relative speed between the two reactants.

$$\begin{aligned} S_{\rm AB}(E) &= 0 && \text{for } E \le E_{\rm a}\,, \\ &= \pi\sigma_{\rm AB}\left(\tfrac{E-E_{\rm a}}{E}\right) && \text{for } E > E_{\rm a}\,. \end{aligned} \tag{28}$$

Using the modified cross-section, the rate becomes

$$k_{\rm nn} = \pi\sigma_{\rm AB}\left(\frac{8}{\pi\mu_{\rm AB}(kT)^3}\right)^{1/2}\int_{E_{\rm a}}^{\infty}(E-E_{\rm a})\,{\rm e}^{-\frac{E}{kT}}\,dE = \pi\sigma_{\rm AB}\left(\frac{8kT}{\pi\mu_{\rm AB}}\right)^{1/2}{\rm e}^{-E_a/kT}. \tag{29}$$

The probability for a Maxwellian gas at temperature $T$ to overcome a barrier of energy $E_{\rm a}$ is $\exp(-E_{\rm a}/kT)$, hence an extra term in the rate coefficients. Higher activation energy implies that the reactants need more energy to start than a reaction with a lower activation energy. Assuming standard values for $\sigma_{\rm AB}$ and $\mu_{\rm AB}$, the rate in the hard-sphere model is

$$k_{\rm nn} \sim 9\times10^{-10}(T/300)^{1/2}{\rm e}^{-E_a/kT}. \tag{30}$$

Using the $\sigma_{\rm AB} = b_{\rm m}^2$, another estimate of neutral-neutral reaction rates is possible

$$k_{\rm nn} \sim 4.8\times10^{-11}(T/300)^{1/6}{\rm e}^{-E_a/kT}. \tag{31}$$

In summary, reaction rate coefficients of neutral-neutral reactions often follow the Arrhenius form

$$k = a(T/300)^b{\rm e}^{-c/T}\,, \tag{32}$$

where $a$ is of the order of $10^{-12}-10^{-10}$, $b$ of the order of unity and should have a value of 0.5 for a perfect gas, and $c$ is the activation energy. A neutral-neutral reaction can be globally exothermic ($\Delta E > 0$) but still has a barrier. For an endothermic reaction, the activation energy should be at least the energy needed to form the products ($c > -\Delta E$). Table 3 provides a few examples of neutral-neutral reactions.

Most rates are measured at ambient temperature (300 K) or higher and extrapolation to lower temperatures is questionable. Indeed quantum mechanical effects can enhance chemical rates. Slow reaction channels with no activation barrier are possible at low temperature, especially when hydrogen tunneling can play a role. Also at 300 K, low-lying excited state can be populated, which can enhance the speed of the reaction. The forward $k_{\rm f}$ and backward $k_{\rm b}$ reaction rate coefficients are related by the equilibrium constant $K$,

$$K = \frac{k_{\rm f}}{k_{\rm b}}{\rm e}^{(\Delta E/kT)}\,. \tag{33}$$

The constant $K$ can be derived from thermodynamics. Besides in protoplanetary disks, neutral-neutral reactions also contribute significantly to the chemistry of planetary atmospheres.

## 6 Destruction of bonds and ionization

The formation and rearrangement of bonds can lead to molecular complexity. On the other hand many energetic processes in space in general and in protoplanetary disks in particular can destroy molecules back to atomic species. The following sections discuss briefly the different destruction processes.

**Table 3.** Parameters $a$, $b$ and $c$ for a few examples of neutral-neutral reactions taken from the UMIST 2006 database; $b$ is dimensionless.

| Reaction | $a$ [cm$^3$ s$^{-1}$] | $b$ | $c$ [K] |
|---|---|---|---|
| H·+·Ö-H ⟶ O + $H_2$ | $7.0\times10^{-14}$ | 2.8 | 1950 |
| H + $\dot{C}H_4$ ⟶ $CH_3$ + $H_2$ | $5.9\times10^{-13}$ | 3.0 | 4045 |
| H + $NH_3$ ⟶ $NH_2$ + $H_2$ | $7.8\times10^{-13}$ | 2.4 | 4990 |
| H + $H_2CO$ ⟶ HCO + $H_2$ | $4.9\times10^{-12}$ | 1.9 | 1379 |
| H-H +:C≡N:⟶ H-C≡N:+ H | $4.0\times10^{-13}$ | 2.9 | 820 |
| C + OH ⟶ CH + O | $2.3\times10^{-11}$ | 0.5 | 14800 |
| C + OH ⟶ CO + H | $1.0\times10^{-10}$ | 0.0 | 0 |
| Ċ +:N-H ⟶ N + CH | $1.7\times10^{-11}$ | 0.5 | 4000 |
| ·C-H + O ⟶ OH + C | $2.5\times10^{-11}$ | 0.0 | 2381 |
| :Ȯ·+·C̈-H ⟶ CO + H | $6.6\times10^{-11}$ | 0.0 | 0 |
| $\dot{C}H$ + $O_2$ ⟶ HCO + O | $1.4\times10^{-11}$ | 0.7 | 3000 |
| CH + $N_2$ ⟶ HCN + N | $5.6\times10^{-13}$ | 0.9 | 10128 |
| $CH_3$ + OH ⟶ $CH_4$ + O | $3.3\times10^{-14}$ | 2.2 | 2240 |
| N + HCO ⟶ CO + NH | $5.7\times10^{-12}$ | 0.5 | 1000 |
| N + HNO ⟶ $N_2O$ + H | $1.4\times10^{-12}$ | 0.5 | 1500 |
| N + $O_2$ ⟶ NO + O | $2.3\times10^{-12}$ | 0.9 | 3134 |
| NH + CN ⟶ HCN + N | $2.9\times10^{-12}$ | 0.5 | 1000 |
| NH + OH ⟶ $NH_2$ + O | $2.9\times10^{-12}$ | 0.1 | 5800 |
| NH + O2 ⟶ HNO + O | $6.9\times10^{-14}$ | 2.7 | 3281 |
| O + CN ⟶ CO + N | $4.4\times10^{-11}$ | 0.5 | 364 |
| O + HCN ⟶ CO + NH | $7.3\times10^{-13}$ | 1.1 | 3742 |
| O + $C_2H_4$ ⟶ $H_2CCO$ + $H_2$ | $5.1\times10^{-14}$ | 1.9 | 92 |
| OH + OH ⟶ $H_2O$ + O | $1.7\times10^{-12}$ | 1.1 | 50 |
| $O_2$ + SO ⟶ $SO_2$ + O | $1.1\times10^{-14}$ | 1.9 | 1538 |
| :N̈·+·C≡C-H ⟶ $C_2N$ + H | $5.0\times10^{-11}$ | 0 | 0 |

### 6.1 Photo-ionization and photo-dissociation

Bond energies of molecules are of the order of 5 – 10 eV corresponding to wavelengths of ≃ 3000 Å and shorter (the far-UV regime, FUV). The theory of photodissociation is well discussed in van Dishoeck et al. (2006). Here only a brief overview is provided. Photodissociation reactions can occur different ways (see Fig. 5).

**Direct photodissociation** (e.g. $H_2^+$, $CH^+$, NH, $H_2O$): The dissociation occurs through a transition to the continuum of a repulsive electronic excited state with respect to the nuclear coordinate. Since spontaneous emission back to the ground state is a comparatively slow process (typical Einstein-A coefficients of $10^9$ s$^{-1}$ for an electronic transition compared with dissociation times of $10^{13}$ s$^{-1}$), almost all absorptions lead to dissociation of the molecule. The photodissociation cross-section has a pseudo-continuum shape.

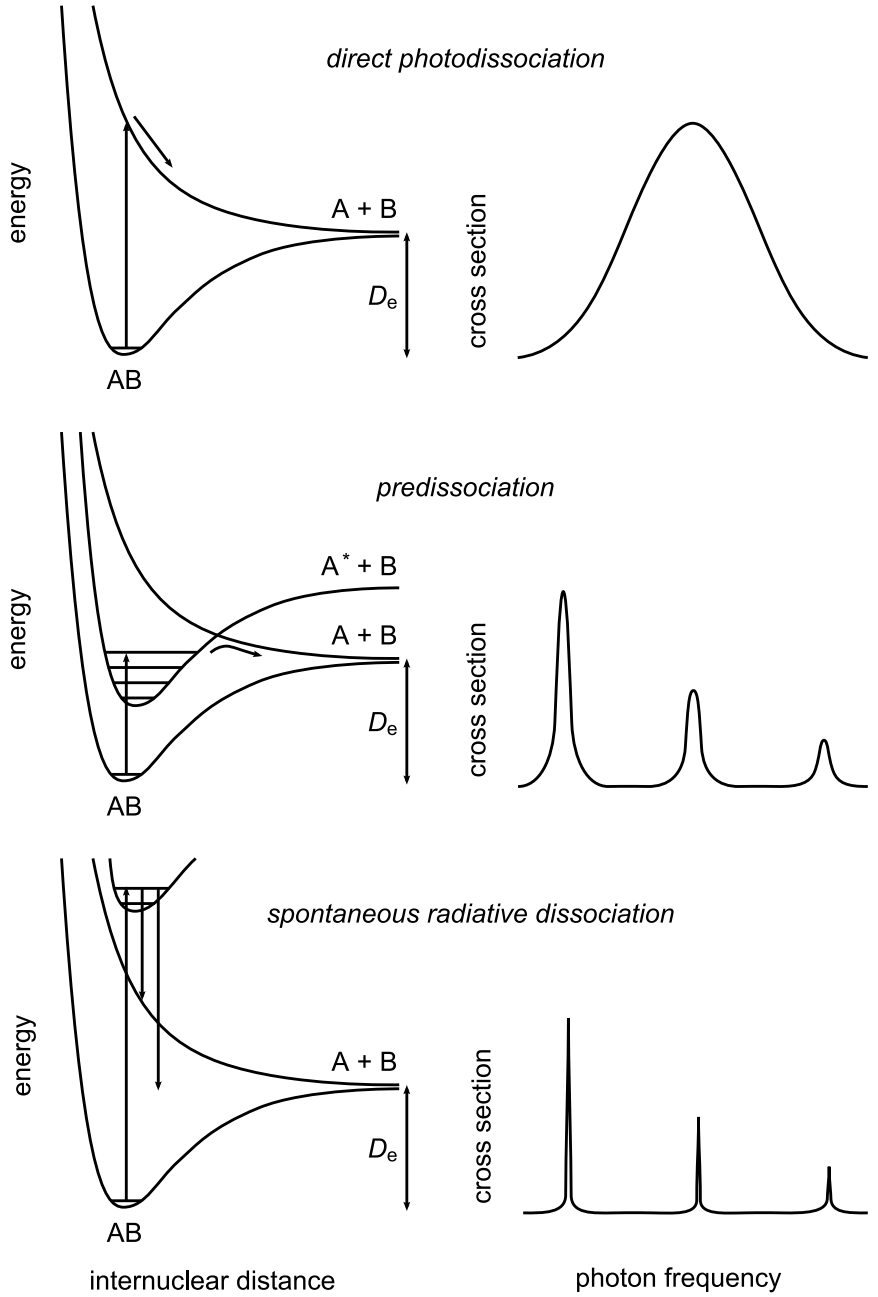


**Figure 5.** Photodissociation processes of diatomic molecules and corresponding cross sections. From top to bottom: direct photodissociation, predissociation and spontaneous radiative dissociation (E. van Dishoeck personal communication).

**Predissociation** (e.g. CO): The dissociation occurs by discrete (line) absorptions into bound electronic states followed by radiation-less coupling with the continuum of a dissociative state of different symmetry. The cross-section is a composition of line absorption profiles.

**Photodissociation through coupled states** (e.g. CH, OH): The dissociation starts with the absorption of a photon to a discrete electronic state followed by a radiation-less coupling with the continuum of a final repulsive state of the same symmetry, which does not cross the bound state. This process can play an important role when Rydberg-valence interactions forbid excited states to cross. The cross-section is composed of a series of resonances superposed on a continuum absorption.

**Spontaneous radiative dissociation** ($H_2$): The bound excited state can decay by spontaneous emission into lower-lying continuum states. The cross section shows narrow discrete absorption Lorentzian profiles with widths determined by the natural radiative lifetimes of the electronic levels. Since the lifetime of electronic levels are short, their natural width is correspondingly relatively large.

Molecular hydrogen photodissociation proceeds via this path. The ground electronic state contains 14 vibrational levels, plus a continuum of levels with $E > \Delta E_{\rm diss} = 4.48$ eV, the molecules binding energy. Hydrogen molecules absorb UV photons in the range $912-1100$ Å into the bound Lyman ($B^1$ and $X^1$ states) and Werner ($C^1$ and $X^1$ states) systems (Fig. 6). Fluorescence to the vibrational continuum of the ground electronic state occurs 10 to 15% of the time (i.e. the molecule is dissociated). In order to dissociate, the molecule must decay from an excited electronic state to a vibrational continuum level lying above the $v = 14$ level in the ground state. The rest of the time $H_2$ relaxes to a bound vibrationally-excited ground electronic state $H_2(v > 1)$. Because the absorption occurs by line absorptions, the optical-depths increase with increasing column of $H_2$ and the photodissociation efficiency decreases. The phenomenon is called $H_2$ photodissociation self-shielding. When the absorption line gaussian core is saturated, further absorption can still occur in the extended Lorentzian wings. At high optical depths, the line wings start to overlap with each other resulting in pseudo-band absorptions. Interestingly, $H_2$ an CO UV absorption line frequencies can be realtively close such that the $H_2$ absorption can also shield CO. This phenomenon is called mutual shielding.

The rate of photodissociation $k_{\rm pd}$ of a molecule by absorption from a lower level $\ell$ into a continuous upper channel $u$ is

$$k_{\rm pd}^{\rm cont} = \int_{\lambda_{\rm H}}^{\lambda_{\rm d}} \sigma(\lambda)\, I(\lambda)\, d\lambda \ \ {\rm s}^{-1} \tag{34}$$

where $\sigma$ is the cross section for photodissociation in cm$^2$ and $I$ is the mean intensity of the radiation in photons cm$^{-2}$ s$^{-1}$ Å$^{-1}$ as a function of wavelength $\lambda$ in Å. The integration runs from the hydrogen photo-ionization limit ($\nu_{\rm H}$) (higher energy photons are completely absorbed by atomic hydrogen) to the dissociation limit ($\nu_{\rm d}$) (the photon has to be energetic enough to break the chemical bonding). For the indirect processes of predissociation and spontaneous radiative dissociation, the rate of dissociation by absorption into a specific level of a bound upper state $u$ from lower level $\ell$ is

$$k_{\rm pd}^{\rm line} = \frac{\pi e^2}{mc^2} \lambda_{u\ell}^2\, f_{u\ell}\, \eta_u\, x_\ell\, I(\lambda_{u\ell}) \ \ {\rm s}^{-1}, \tag{35}$$

where $f_{u\ell}$ is the oscillator strength, $\eta_u$ is the dissociation efficiency of the upper level (between 0 and 1), and $x_\ell$ is the fractional population in level $\ell$. In that case, the photodissociation rate depends not only on strength of the UV field but also on the local gas temperature and density. The branching ratios between photodissociation products are not well determined except for small molecules. Cross-sections are typically between 0.01 and $0.1 \times 10^{-16}$ cm$^2$ when dipole-allowed transitions are available.

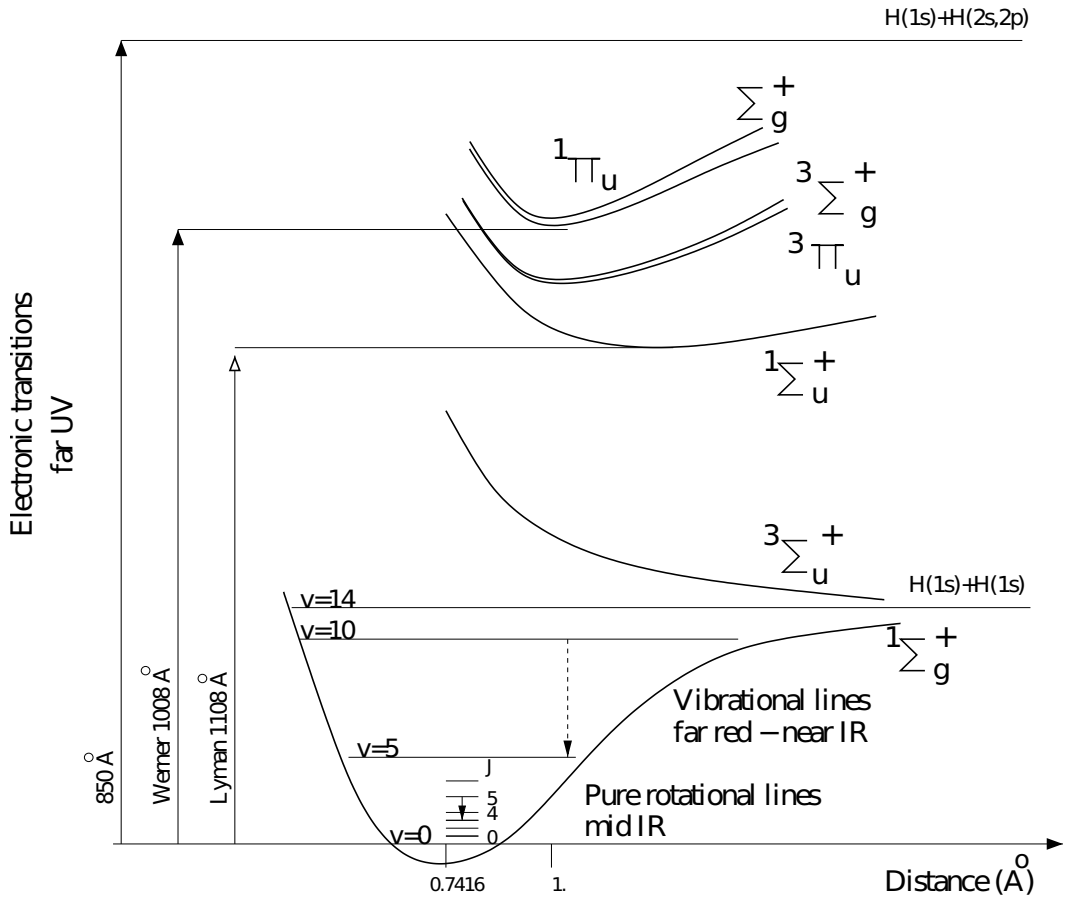


**Figure 6.** $H_2$ energy curves (S. Cazaux).

Interstellar UV radiation fields are often normalized to the standard local average value corresponding to the so-called Draine or Habing field ($I_{\rm UV,ISM} \sim 10^8$ FUV photons cm$^{-2}$ s$^{-1}$ sr$^{-1}$, Fig. 7). This translates to photodissociation rates for a standard FUV field $I_{\rm UV,ISM}$ of $10^{-9} - 10^{-10}$ s$^{-1}$. At the surface of protoplanetary disks at 1 AU, the UV field can reach up to $\chi = 10^6 - 10^7$ $I_{\rm UV,ISM}$.

### 6.2 Dissociative recombination reactions

Dissociative recombination (DR) reactions involve the capture of an electron by a molecular ion to form a neutral species in an electronic doubly excited, usually strongly repulsive, state located above the first ionization potential, which subsequently dissociates ($AB^+ + e \rightarrow AB^{**} \rightarrow A+B$). The rates are large ($10^{-7}$ s$^{-1}$) because of the long-range electrostatic potential between a cation and an electron and of the low mass of the electron. The rates vary in the range of $T^{-1/3}$ to $T^{-1}$. Dissociative electron recombination reactions are the final reactions leading to many neutral molecules at low temperatures and the second species is often atomic or molecular hydrogen. An example is the sequence leading to

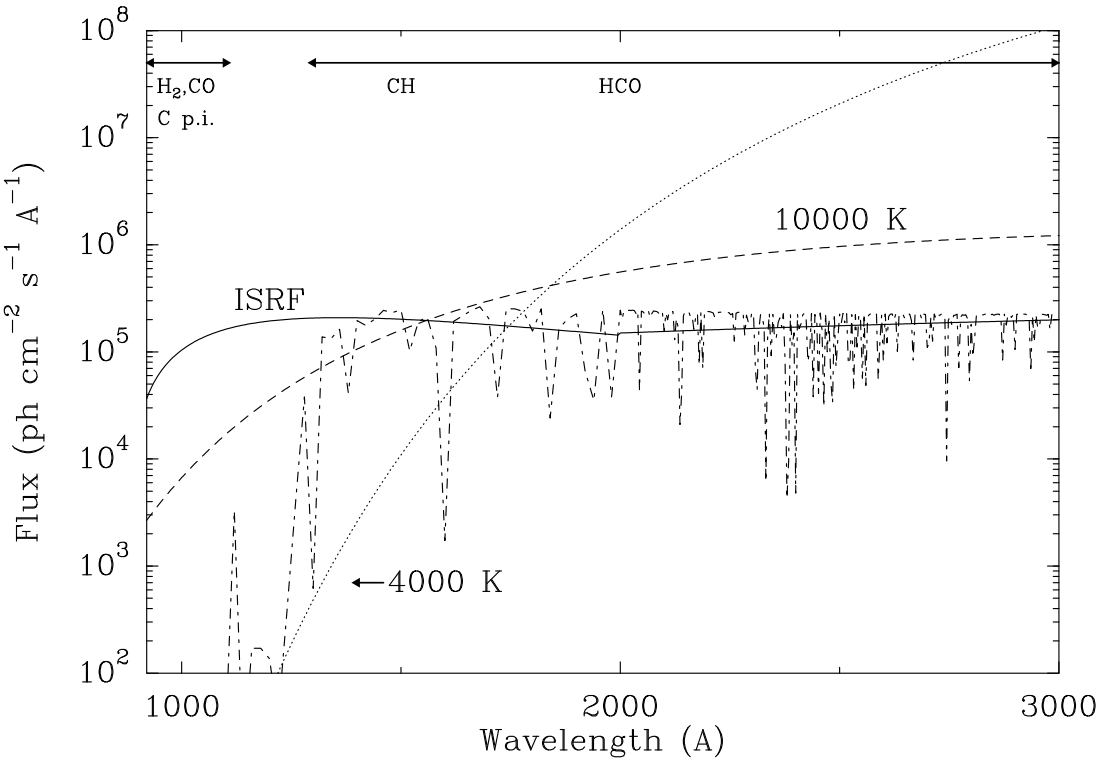


**Figure 7.** Comparison of the general interstellar radiation field of Draine extended for $\lambda > 2000$ Å with various black body radiation fields. Reproduced from van Dishoeck et al. (2006) with permission of The Royal Society of Chemistry.

the formation of water starting with $H_3^+$:

$O + H_3^+ \rightarrow OH^+ + H_2$
$OH^+ + H_2 \rightarrow H_2O^+ + H$
$H_2O^+ + H_2 \rightarrow H_3O^+ + H$
$H_3O^+ + e^- \rightarrow H_3O^{**} \rightarrow H_2O + H$

The three first steps are ion-neutral reactions, which compete themselves with dissociative recombination reactions (e.g. $H_2O^+ + e^- \rightarrow O + H + H$). Table 4 gives a sample of important dissociative recombination reactions. One can notice for example that the branching ratio in the recombination reaction of $H_3O^+$ favors OH as product instead of $H_2O$. Dissociative recombination reactions are also key intermediate reactions leading to abundant species such as CO:

$C + H_3^+ \rightarrow CH^+ + H_2$
$CH^+ + H_2 \rightarrow CH_2^+ + H$
$CH_2^+ + e^- \rightarrow CH + H$
$CH + O \rightarrow CO + H$

Another important role is that DR reactions are efficient neutralizing agents. The importance of these reactions stresses the need to understand the electron abundance in protoplanetary disks. If

electrons are locked onto grain surfaces, the recombination reactions are much slower because charges on grains move much more slowly. Although the rate coefficients are known accurately, the product branching ratios can be highly uncertain. However, products with strong bonds are usually preferred.

**Table 4.** Parameters for a few examples of dissociative electron recombination reactions.

| Reaction | $a$ [cm$^3$ s$^{-1}$] | $b$ |
|---|---|---|
| $H_2^+ + e^- \longrightarrow H + H$ | $1.6 \times 10^{-8}$ | -0.43 |
| $H_2O^+ + e^- \longrightarrow O + H + H$ | $3.1 \times 10^{-7}$ | -0.5 |
| $H_2O^+ + e^- \longrightarrow OH + H$ | $8.6 \times 10^{-8}$ | -0.5 |
| $H_3O^+ + e^- \longrightarrow OH + H_2$ | $6.0 \times 10^{-8}$ | -0.5 |
| $H_3O^+ + e^- \longrightarrow O + H + H_2$ | $5.6 \times 10^{-9}$ | -0.5 |
| $H_3O^+ + e^- \longrightarrow OH + H + H$ | $2.58 \times 10^{-7}$ | -0.5 |
| $H_3O^+ + e^- \longrightarrow H_2O + H$ | $1.08 \times 10^{-7}$ | -0.5 |
| $H_3^+ + e^- \longrightarrow H_2 + H$ | $2.3 \times 10^{-8}$ | -0.52 |
| $HCN^+ + e^- \longrightarrow CN + H$ | $2.0 \times 10^{-7}$ | -0.5 |
| $HCO^+ + e^- \longrightarrow CO + H$ | $2.4 \times 10^{-7}$ | -0.69 |
| $HNO^+ + e^- \longrightarrow NO + H$ | $3.0 \times 10^{-7}$ | -0.69 |
| $C_2^+ + e^- \longrightarrow C + C$ | $3.0 \times 10^{-7}$ | -0.5 |
| $CH^+ + e^- \longrightarrow C + H$ | $1.5 \times 10^{-7}$ | -0.42 |
| $CH_2^+ + e^- \longrightarrow CH + H$ | $1.4 \times 10^{-7}$ | -0.55 |
| $CH_2^+ + e^- \longrightarrow C + H + H$ | $4.0 \times 10^{-7}$ | -0.6 |
| $CH_3^+ + e^- \longrightarrow CH + H + H$ | $2.0 \times 10^{-7}$ | -0.4 |
| $CH_3^+ + e^- \longrightarrow CH + H_2$ | $2.0 \times 10^{-7}$ | -0.5 |
| $CH^+ + e^- \longrightarrow C + H$ | $1.5 \times 10^{-7}$ | -0.42 |
| $CN^+ + e^- \longrightarrow C + N$ | $1.8 \times 10^{-7}$ | -0.5 |
| $NH_4^+ + e^- \longrightarrow NH_2 + H_2$ | $1.5 \times 10^{-7}$ | -0.47 |
| $NO_2^+ + e^- \longrightarrow NO + O$ | $3.0 \times 10^{-7}$ | -0.5 |
| $OH^+ + e^- \longrightarrow O + H$ | $3.8 \times 10^{-8}$ | -0.5 |
| $OCS^+ + e^- \longrightarrow CS + O$ | $4.9 \times 10^{-8}$ | -0.62 |

### 6.3 Collisional dissociation

Molecules are destroyed by collisions whose energy is higher than the bond energy. Such a process is especially efficient in high temperature environments (several thousands of Kelvin), where the colliding partners have sufficient kinetic energy to excite vibrational levels that are higher than the dissociation continuum of the molecule. Main contributors to collisional dissociations are H, He and $H_2$, i.e. the most abundant species.

### 6.4 Non-LTE effects on reaction rates

The discussion so far has assumed that all the degrees of freedom are in equilibrium and can be described by a single temperature corresponding to the kinetic temperature of the gas. In many circumstances, the internal degrees of freedom are not at LTE. Molecular hydrogen is formed in highly vibrationally excited levels and can be excited by absorption of UV photons. The vibrational energy

levels of $H_2$ can be larger than many activation barriers. It is however not clear how much of the internal energy can be used to overcome the barriers (Agúndez et al. 2010). The interaction of atoms such as O, C, or Si with neutral radicals is due to long-range atomic quadrupole forces, which can overcome the barriers in the potential energy surfaces that result from chemical interactions at intermediate separations. The reactivity is determined by the quadrupole moment of the lowest spin-orbit states and is therefore sensitive to the population of the fine-structure levels. The rate coefficients can then be enhanced by an order of magnitude at low temperature if the atoms are electronically excited upon the absorption of a UV photon for example. The last category of non-LTE effects are differences in rate coefficients due to different hydrogen spin (ortho or para, Hugo et al. 2009).

## 7 Grain surface reactions

Dust grains increase at the same time the probability of encounters between adsorbed species and act as a "third" body to receive most of the heat generated by exothermic reactions. Part of the excess energy can be imparted to break the bond between the newly formed species and the surface leading to the escape of the species to the gas-phase, and part can be used by the species to diffuse rapidly on the surface. The exact fractions of the energy given to each process are still under study by experimental and theoretical chemists.

Grain-surface processes are paramount to the formation of some common molecules, including $H_2$ along with that of more complex molecules. Grain surface chemistry is governed by the accretion/desorption rates as well as the surface migration rates. Those rates will depend on the nature and geometry of the dust grains. Fig. 8 provides an overview of the chemical coupling between gas and surfaces and the various types of processing occurring on grains. The discussion of grain surface chemistry is heavily based on the textbook by Tielens (2010).

### 7.1 Freeze-out and desorption processes

Dust grains are much heavier than atoms and molecules and we can assume that the barycenter of the system is located at the center of the grain. The adsorption rate is

$$k_{\rm ads} = n_{\rm d}\langle\sigma_{\rm d}v\rangle S_{\theta=0}(T,T_{\rm d})\ {\rm s}^{-1}, \tag{36}$$

where $n_{\rm d}$ is the number density of dust grains, $\sigma_{\rm d}$ is the geometric cross-section for a compact grain of radius $a$ ($\sigma_{\rm d}=\pi a^2$), $v$ the velocity of the gas, $\langle\sigma_{\rm d}v\rangle$ the velocity-averaged cross-section. Upon arrival at the surface, the particle has to dissipate its excess energy ($E_i = 1/2\,kT$ for an atom or $E_i = 3/2\,kT$ for a molecule) before it can stick. Hollenbach & Salpeter (1970) defined the sticking coefficient for zero-coverage as

$$S_{\theta=0} = \int_0^\infty \epsilon\,{\rm e}^{-\gamma\epsilon}P(\epsilon)\,d\epsilon \Big/ \int_0^\infty \epsilon\,{\rm e}^{-\gamma\epsilon}\,d\epsilon, \tag{37}$$

where $P(\epsilon)$ is the adsorption probability for a particle after $n_{\rm h}$ hops where $n_{\rm h}$ is the number of hops needed for the particle to give all its excess energy to the surface ($n_{\rm h}\sim E_i/\Delta E_s$, where $\Delta E_s$ is the amount of energy transfer at each hop and would be defined later), $T$ is the gas temperature, and $\gamma\equiv E_c/kT$. The variable $\epsilon$ is defined as $\epsilon = E_i/E_c$, $E_c = \Omega(E_{\rm ads}\Delta E_s)^{1/2}$. $\Omega$ is between 1 (Lambert's law) to 2 (isotropic scattering). The formula can be approximated when $kT_{\rm d}\ll E_{\rm ads}$ by

$$S_{\theta=0} \simeq (\gamma^2+0.8\gamma^3)/(1+2.4\gamma+\gamma^2+0.8\gamma^3). \tag{38}$$

A simple approximation of $\Delta E_s$ in a head-on collision in the hard-sphere approximation is given by the Baule expression $\Delta E_s = 4\mu/(1+\mu)^2 E_i$, where $\mu = m_{\rm gas}/M_{\rm surf}$ ($m_{\rm gas}$ is the mass of the impinging species

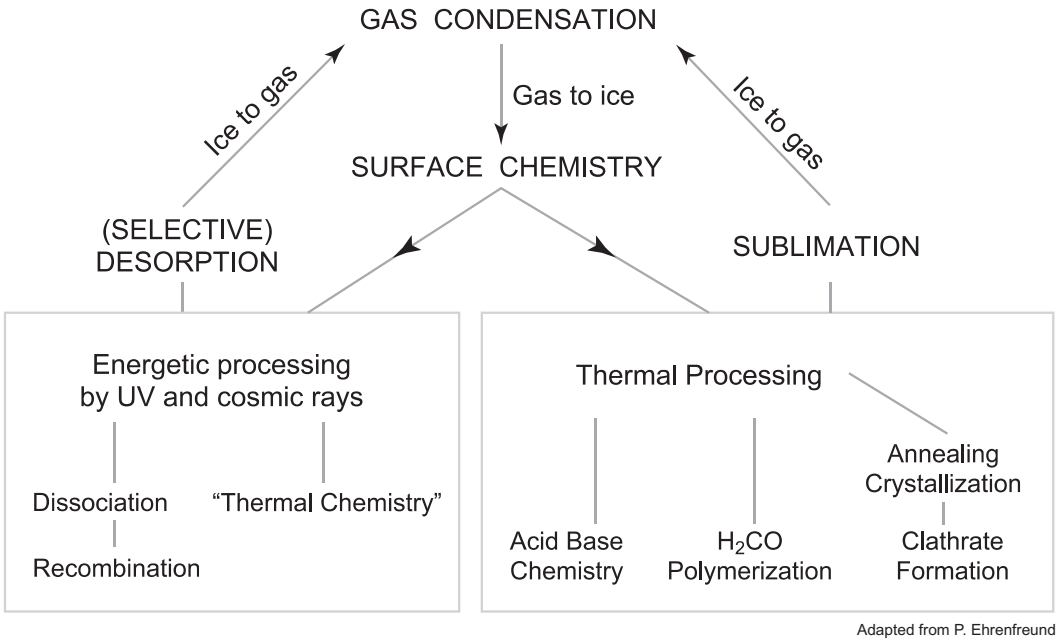


**Figure 8.** Gas-grain chemical processes (after P. Ehrenfreund).

and $M_{\rm surf}$ is the mass of the species at the surface). Another possibility is the expression proposed by Hollenbach & Salpeter (1970) $\Delta E_s = \mu(E_i + E_{\rm ads})$. The expressions are strictly valid up to $\mu$ =1. For an atomic hydrogen atom hitting a water surface, we can estimate $\mu$=1/16 and $\Delta E_s$(Baule) $\simeq 0.22 E_i = 0.11\,kT$. Alternatively, $\Delta E_s$(HS) = $(1/16)(0.5\,kT + (3/4)E_{\rm ads})$. Assuming an adsorption energy $E_{\rm ads}$ of 600 K and $\Omega = 2$, the formula recovers recent model-results by Veeraghattam et al. (2014). In the particular case of H sticking on silicate or amorphous ice surfaces, many experimental and theoretical studies have been performed. For example, Chaabouni et al. (2012) propose a parametric formula that fits experimental and theoretical values

$$S_{\theta=0}(T) = S_0(1 + \beta T/T_0)/(1 + T/T_0)^{\beta}, \tag{39}$$

where $\beta = 2.5$ (isotropic gas flux), $S_0 = 1$ and $T_0 = 25$ and 50 for an adsorption of atomic hydrogen on silicate and amorphous ice surface respectively (although a value of 104 instead of 50 would fit better the most recent simulations).

Before sticking, a particle will hop a few times between adsorption sites. Therefore the sticking coefficient is intimately related to the thermal accommodation coefficient $\alpha_{\rm T}$. The site hopping competes with desorption back to the gas and not all particles will stick to the grain at the end. The process is captured in the sticking coefficient $S_{\theta=0}(T, T_{\rm d})$, which is the probability for a particle to thermally equilibrate with the surface, becoming finally adsorbed at the surface after a few hops between adsorption sites. It is defined as the ratio between the rate of adsorption on the surface to the impinging rate. The sticking coefficient depends on the nature of the accreting species, the gas kinetic temperature $T$, the dust temperature $T_{\rm d}$, the excitation of the phonon spectrum of the grain, and the interaction energy of the species and the surface, which varies with the nature of the surface, and is generally close to 1. Besides those already discussed, other empirical formula exist that take theoreti-

cal and experimental considerations into account. Unfortunately there exists no data on grain surface temperature dependence, because the surface in most studies was kept at 10 K. However, the surface temperature is an important parameter controlling the sticking, especially for disk chemical modeling where a large range of gas and dust temperature are possible. The analytical formula

$$S_{\theta=0}(T, T_{\rm d}) = \left[1 + 4 \times 10^{-2}(T + T_{\rm d})^{1/2} + 2 \times 10^{-3} T + 8 \times 10^{-6} T^2\right]^{-1}, \tag{40}$$

which has been used by Hollenbach & McKee (1979), is based on the seminal work by Burke & Hollenbach (1983) which takes the effects of warm grain surfaces into account. The sticking coefficient formula is for zero-coverage ($\theta = 0$). At non-zero coverage, the number of available sites for hopping decreases and a correction term to the sticking coefficient has to be applied. The general form for the sticking coefficient becomes

$$S(T, T_{\rm d}) = S_{\theta=0}\left(1 - \frac{\theta}{\theta_{\rm sat}}\right)^n, \tag{41}$$

where $\theta_{\rm sat}$ and $n$ are fitting parameters to experimental data. Theoretically $n$ is 1 for physisorption, but many experiments show that the value is greater than one in many cases. For simplicity, we assume from now that $S(T, T_{\rm d}) = S_0(1 - \theta)$ with ($S_0 = S_{\theta=0}$). Interestingly, the excess energy carried by the impinging particle can also be used to overcome reaction activation barriers but no detailed study has quantified this effect yet.

The binding (adsorption) of a particle to a surface is considered either as chemisorption or as physisorption depending on the energy of the bonds (Fig. 9). The nature and strength of chemisorption bonds are similar to the bonding of atoms in molecules (adsorption energy $E_{\rm ads} > 0.5$ eV/particle, 1 eV $\simeq$ 5802 K). Physisorption involves only van der Waals interaction (polarization) between the surface and the particle. A simple estimate of the adsorption energies can be obtained by summing independently the van der Waals interactions between the particle and the atoms at the grain surface. Physisorption well depths have energies between 0.01 and 0.2 eV. The geometry of the surface is important. A perfectly flat crytalline surface or a rough irregular surface will bind differently to particles. The adsorption energy can also be influenced by the presence of adsorbates on the surface that can strengthen or weaken the surface bond. The adsorption to a chemisorption site involves hopping over a few physisorption sites (Kisliuk's model of chemical adsorption).

The presence of a permanent dipole moment of the gas particle can increase the adsorption energy because physisorptions are mostly due to van der Waals interactions. The coverage of the surface by a layer of water ice will prevent further chemisorptions and only adsorptions on physisorbed sites will be possible. Once covered by a water ice layer, atomic and molecular hydrogen will constantly adsorb and desorb from the surface, because as $H_2$ coverage increases, the number of available adsorption sites (water ice dangling H and O sites) decreases. Not all adsorption energies for all species on all type and nature of surfaces are known. The residence time of a species on a grain surface is the time required by the species to gain sufficient energy by thermal fluctuation to overcome the adsorption energy and is given by

$$\tau_{\rm des} = \nu_0^{-1} \exp(E_{\rm ads}/kT_{\rm d}), \tag{42}$$

where $\nu_0$ is the vibrational frequency of the adsorbed species. Consider a species of mass $m$ adsorbed with an energy $E_{\rm ads}$ on a surface with a number density of surface sites $N_{\rm s}$ ($\simeq 1.5 \times 10^{15}$ cm$^{-2}$). For a symmetric harmonic potential, the frequency of an atomic adsorbed species in the surface site is

$$\nu_z = \left(\frac{2 N_{\rm s} E_{\rm ads}}{\pi^2 m}\right)^{1/2} \tag{43}$$

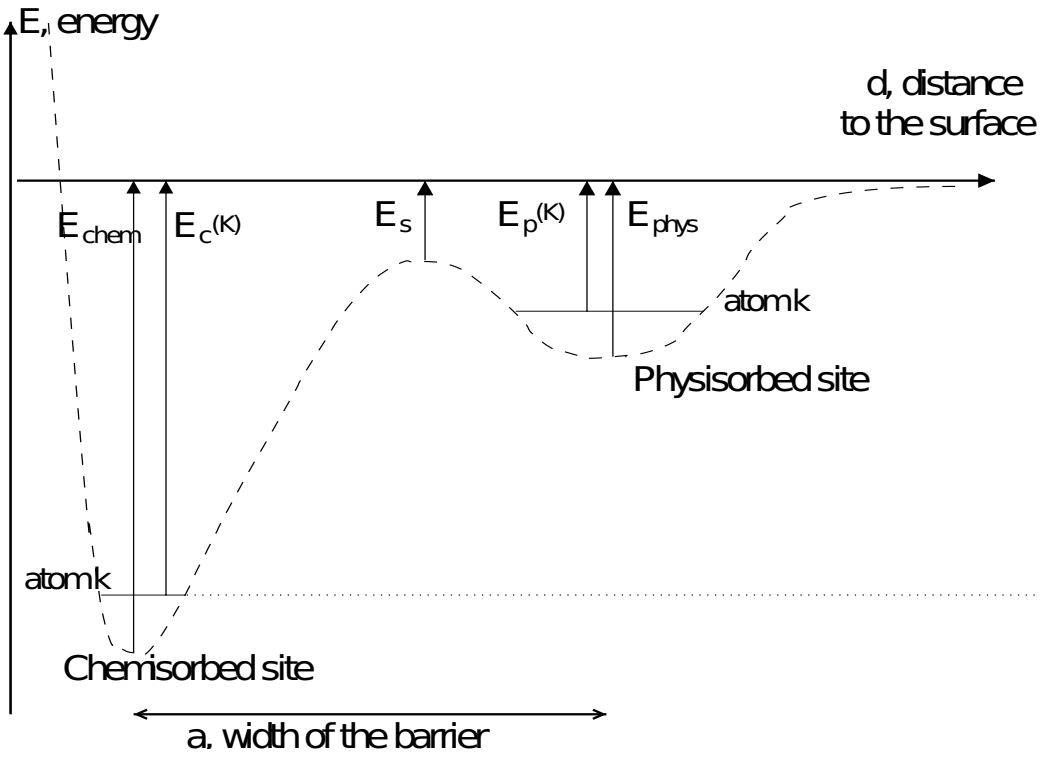


**Figure 9.** Surface binding energy curve (S. Cazaux).

An adsorbed species has replaced one degree of translational freedom by a vibrational degree of freedom of the bond with the surface. For a monoatomic gas that is completely mobile on the surface,

$$\nu_0 = \frac{\alpha}{1-\alpha\theta}\frac{kT}{h}f_z^{-1}S = \frac{kT}{h}\left(1-\mathrm{e}^{-h\nu_z/kT}\right)S_0, \tag{44}$$

where $f_z$ is the vibrational partition function of the adsorbate in the mode perpendicular to the surface. We have assumed that $\alpha$, the number of species per adsorption site, is one. When this mode is fully excited (e.g. high temperatures, $h\nu_z \ll kT$), $\nu_0 \simeq \nu_z S_0$. At low temperatures, when the surface bonding mode is not excited at all, $f_z = 1$ and $\nu_0$ is $kT/h = 2\times10^{11}(T/10\ \mathrm{K})\ \mathrm{s}^{-1}$, with a sticking coefficient of one. When the species is not mobile on the surface, $\nu_0$ has to be modified to

$$\nu_0 = \frac{kT}{h}\frac{1}{f_x f_y f_z}\frac{2\pi mkT}{N_s h^2}S_0 \tag{45}$$

where $f_x$, $f_y$, and $f_z$ are the partition functions in the $x$, $y$, and $z$ (perpendicular to the surface) direction and the last factor takes into account the number of possible ways in which adsorbates can be distributed over the surface sites. This is a situation that is appropriate for CO on an ice surface. For an immobile species with $m = 30$ atomic mass units, we find at 10 K, $\nu_0 = 1.4\times10^{12}\ \mathrm{s}^{-1}$. Both

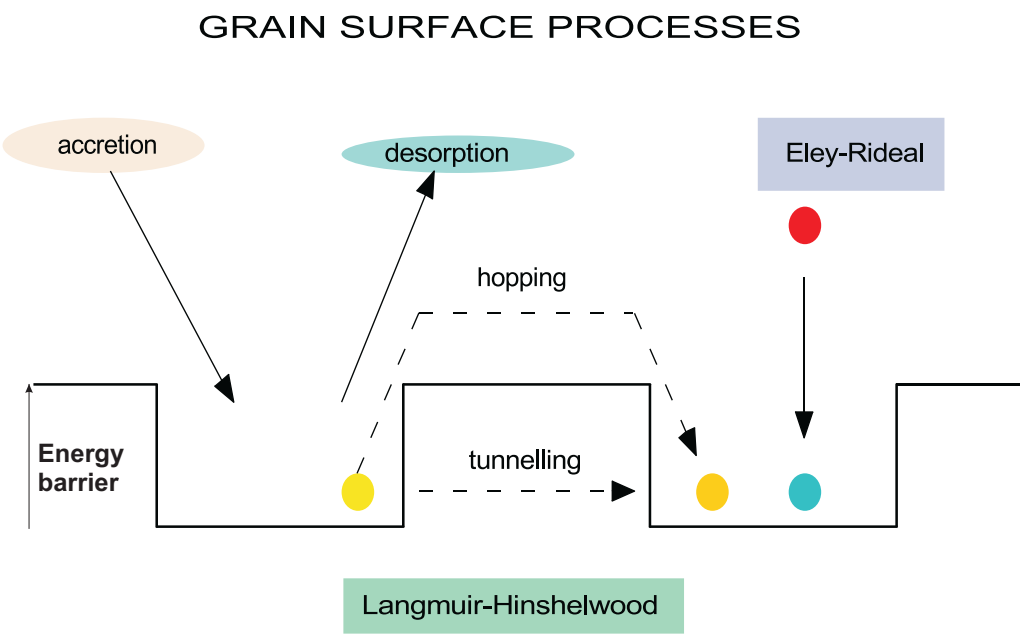


**Figure 10.** Surface chemistry processes

the adsorption energy of atomic and molecular hydrogen depend on the surface coverage by $H_2$. The atomic hydrogen evaporation rate and the accretion rate of molecular hydrogen are coupled. For surface temperatures below 19 K, the evaporation/desorption timescale for atomic H is independent of the temperature and is given by

$$\tau_{\rm des} = 3 \times 10^2 \frac{n_{\rm H}}{10^4\ {\rm cm}^{-3}}\ {\rm s}. \tag{46}$$

Species can also desorb by photodesorption in which the absorption of an energetic photon can provide sufficient energy for a species to overcome the energy of the adsorption well. Photodesorption yields are estimated to be around $10^{-3}$.

### 7.2 Mobility on grain surfaces

Once on grain surfaces, the particles can either desorb or move between adsorption sites. Three different kinds of motion on the surface can be considered: (a) a transition between a physisorbed site and a chemisorbed site, (b) a transition from a chemisorbed site to another chemisorbed site, and (c) a transition from a physisorbed site to another physisorbed site. Heavy elements can hop from sites to adjacent sites with a time scale given by

$$\tau_{\rm diff} = \nu_{\rm diff}^{-1} \exp\left(E_{\rm diff}/kT_{\rm d}\right), \tag{47}$$

where $\nu_{\rm diff}$ is the frequency for vibrational motion parallel to the surface, which is comparable to $\nu_0$. The barrier against migration $E_{\rm diff}$ is typically a third to half of the adsorption energy. Surface

migration is to first order a random walk process in the two dimensional surface. A surface species will visit $N \ln N$ sites in $N$ steps. Thus the number of sites $N_t$ visited by a species before evaporation is $N_t \ln N_t \tau_{diff} = \tau_{ev}$.

The lightest surface particles (H and D) can also migrate through quantum mechanical tunneling, although even for more massive species, tunneling can proceed faster than thermal diffusion at low grain temperature. The shape of the barrier is not known and for simplicity rectangular barriers are assumed. The tunneling time through a rectangular barrier with height $E_{diff}$ and width $a$ is

$$\tau_t = \nu_0^{-1} \exp\left[\frac{2a_t}{\hbar}(2mE_{diff})^{1/2}\right], \tag{48}$$

where $\nu_0$ ($\simeq \nu_{diff}$) is the vibrational frequency of the species in the well and $m$ the mass of the species. The actual shape of the barrier should be used in detailed calculations. For example the barrier for H on an $H_2O$ surface partially covered by $H_2$ is unknown. An estimate for $E_{diff}$ is that it should be less than 350 K. With $\nu_0 = 2 \times 10^{13}$ s$^{-1}$ and $a_t = 1$ Å the migration timescale by tunneling is estimated to be $1.5 \times 10^{-10}$ s for H. It should be noted that the timescale to move $N$ sites away is proportional to $N$ and not $N^2$ as for thermal hopping. We can equate the thermal diffusion with the tunneling diffusion timescale to find the temperature below which tunneling diffusion starts to dominate

$$T_{diff,t} = 24.5 \left(\frac{E_{diff}}{100\ \mathrm{K}}\right)^{1/2} \left(\frac{1\ \text{Å}}{a_t}\right)^{-1/2} N_{atoms}^{-1/2}\ \mathrm{K}, \tag{49}$$

where $N_{atoms}$ is the number of atoms of the species on the surface. For an hydrogen atom, tunneling diffusion dominates at temperatures below 24 K. For molecular hydrogen ($E_{diff} = 0.3 \times 430$ K), it is 19 K, for an oxygen atom ($E_{diff} = 0.3 \times 800$, $N_{atoms} = 16$), the tunneling temperature is 9.5 K. In general, an accreted H atom may be able to pick from among many possible co-reactants. The probability for reaction of atomic H with species $i$ is then given by

$$\Phi_i = \frac{\theta_i p_0(i)}{\sum_j \theta_j p_0(j)} \tag{50}$$

where the summation is over all possible coreactant species. The activation barriers involved have been taken from gas phase studies and their applicability to low temperature grain-surface chemistry is unclear. At low temperatures, grain surfaces have a significant molecular hydrogen coverage ($\simeq 0.2$). Reactions with $H_2$, which have large activation barriers, would also occur via tunneling. The reaction probability is the probability that a species will react with $H_2$ before another migrating radical arrives

$$p_r = \tau_{ar}\, \theta(H_2)\, p_0 \tag{51}$$

The most relevant surface reaction involving $H_2$ is the formation of water by the reaction OH + $H_2$.

## 8 The rate equation treatment of surface reactions

The simplest way to model surface reactions is to include those reactions into a gas-phase chemistry network. The surface reaction rate between a surface species $i$ and a surface species $j$ is (Hasegawa et al. 1992)

$$k_{ij} = \kappa_{ij}(R_{diff,i} + R_{diff,k})/n_d\ \mathrm{cm}^{-3}\ \mathrm{s}^{-1}, \tag{52}$$

where $\kappa_{ij}$ is the probability for the reaction to occur each time the species arrive at a new adsorption site and $n_d$ is the dust particle density. The probability $\kappa_{ij}$ is one when no reaction barrier exists and otherwise takes the form

$$\kappa_{ij} = Q \exp(-E_a/kT_d) \exp(-E_{therm}/kT), \tag{53}$$

with $E_a$ being the activation barrier, and $E_{therm}$ the exothermiticity of the reaction. $R_{diff,i}$ and $R_{diff,j}$ are the surface diffusion rates of species $i$ and $j$, defined as

$$R_{diff,i} = (\tau_{diff,i}^{-1} + \tau_{t,i}^{-1})/N_{site} \tag{54}$$

with $N_{site} = N_s 4\sigma_d$ the number of adsorption sites per grain. Both species can either diffuse thermally or by quantum tunneling. Likewise, species can tunnel through the activation barrier (Fig. 10). R.P. Bell developed the quantum tunneling factor $Q$ that modifies the Arrhenius treatment of reaction with an activation barrier

$$Q = \frac{e^{\alpha}}{\beta - \alpha}\left(\beta\, e^{-\alpha} - \alpha\, e^{-\beta}\right), \tag{55}$$

where $\alpha = E_a/kT_d$ and $\beta = (2a/\hbar)\sqrt{2\mu_m E_{act}}$ with $\mu_m = m_i m_j/(m_i + m_j)$. The advantage of the rate equation approach is that the coupling with gas-phase chemistry is straightforward. The main drawback lies in its limitation to large surface coverages. Other diffusion processes have been invoked like diffusion when a grain is heated after being hit by a cosmic ray. Surface reactions are exothermic and the energy released by the reaction can be used by the nascent species to desorb back into the gas-phase. The Rice-Ramsperger-Kassel theory provides for this process the probability

$$P = (1 - E_{ads}/E_{read})^{3N_{atoms}-6}, \tag{56}$$

where $N_{atoms}$ is the number of atoms in the product molecule. In the form of rate reactions, the branching ratio for desorption products is $f = cP(1 + cP)$ where $c = \nu/\nu_s = 0.01$, the ratio of the surface–molecule bond-frequency to the frequency at which energy is transferred to the grain surface. (Garrod et al. 2007). The value for $c$ is debated and ranges from 0.01 to 0.1 and is related to the mass ratio between the surface molecules and the surface constituents. Photoreactions also occur for grain surface species. Most of the rates are scaled from the gas-phase rates, which is a rough approximation.

We can make an order-of-magnitude estimate of the rate coefficients. We assume no barrier to the reaction and that the diffusion is dominated by tunneling by the hydrogen atom at $T = T_d = 10$ K. The rate coefficient simplifies to

$$k_{ij} \simeq R_{diff,H}/n_d = (4\pi a^2 N_s \tau_{t,H} n_d)^{-1} = 1.37 \times 10^6 (a_{\mu m}/\tau_{t,H} n_H) = 9.13 \times 10^{15} (a_{\mu m}/n_H), \tag{57}$$

where the average number of dust grains in the disk is

$$n_d = \frac{2.2 \text{ amu } n_H}{(4/3)\pi\rho_d a^3 gd} \approx 2.9 \times 10^{-15} n_H \left(\frac{\mu m^3}{a^3}\right)\left(\frac{100}{gd}\right), \tag{58}$$

where $gd$ is the gas-to-dust mass ratio assumed to be 100. We have assumed a silicate mass density of 3.0 g cm$^{-3}$. Garrod & Pauly (2011) have recently suggested that the $\kappa_{ij}$ term should be modified to take the competition with diffusion into account because the rate equation treatment includes the processes of adsorption, desorptions, and reactions explicitly, but not the diffusion $\kappa'_{ij} = f_{reac}\kappa_{ij}$, where

$$f_{reac} = \frac{Q\nu_0 \exp(-E_{act}/kT_d)}{Q\nu_0 \exp(-E_{act}/kT_d) + \tau_{diff,i}^{-1} + \tau_{diff,j}^{-1}}. \tag{59}$$

Applying the formula to our example ($\mu_m = m_i m_j/(m_i + m_j) \simeq m_H$) leads to

$$f_{reac} = \frac{1}{1 + \exp(-2a/\hbar\sqrt{2m_H E_{diff}})} \simeq 0.98. \tag{60}$$

In case of no energy barrier, the correction is minor. If there is a barrier of energy $E_{\rm act} = 1000{-}2500$ K ($> E_{\rm diff} = 100$ K) for the surface reaction CO(s) + H(s) → HCO(s) and if H-tunneling dominates both the reaction efficiency and diffusion, we obtain

$$f_{\rm reac} \simeq \frac{{\rm e}^{-2a/\hbar\sqrt{2m_{\rm H}E_{\rm act}}}}{{\rm e}^{-2a/\hbar\sqrt{2m_{\rm H}E_{\rm act}}} + {\rm e}^{-2a/\hbar\sqrt{2m_{\rm H}E_{\rm diff}}}} = \frac{1}{1 + {\rm e}^{-2a/\hbar\sqrt{2m_{\rm H}}(\sqrt{E_{\rm diff}}-\sqrt{E_{\rm act}})}} \sim 1.5\times10^{-4} - 8.3\times10^{-8}. \quad (61)$$

The rate coefficient is decreased because it is more probable for the hydrogen atom to tunnel to an adjacent site than to tunnel through the reaction barrier. The rate is extremely sensitive to the value of the energy barrier, which is rarely known from experimental studies.

### 8.1 Types of surface reactions

Reactions involving species with unpaired electrons can be expected to occur upon collision on the surface. Of course, this presumes that one of the reactants is mobile on the surface. Thus, specifically, this includes reactions involving H, C, N, or O atoms with themselves or with radicals such as OH, CH, etc. This list is not complete, as longer and longer carbon backbones can be made through the sequential addition of carbon atoms. Also, D-isotopic reactions can be included analogously to those of H atoms.

The unique advantage of grain surface chemistry is the possibility for reactions with activation barrier involving an hydrogen atom to proceed even at low grain surface temperature. The hydrogen atom can quantum mechanically tunnel through energy barriers and as the frequency of encounters of an atomic hydrogen with a surface species is much higher than in the gas phase, there is a non-zero probability that a reaction will proceed by H-atom tunneling. An hydrogen atom located in a surface site can migrate to a neighboring site if it is not occupied or react with the species in this site. The mechanism is called the Langmuir-Hinshelwood mechanism (Fig. 10). If the reaction has an activation barrier $E_{\rm a}$, the reaction probability is

$$p = \frac{p_0}{p_0 + p_{\rm diff}}, \quad (62)$$

where

$$p_0 = \nu_0 \exp\left[-\frac{2a}{\hbar}(2mE_{\rm a})^{1/2}\right] \quad (63)$$

for a rectangular barrier and $p_{\rm diff}$ is the diffusion probability. The reaction probability competes with the migration probability. If the other reactant has a surface coverage $\theta_{\rm r}$, then an hydrogen atom will have $n_{\rm r} = \tau_{\rm ev}/\tau_{\rm diff}\theta_{\rm r}$ tries to react through tunnelling. The probability for a reaction to occur the $k$-th time is $p_k = (1-p)^{k-1}p$. The overall probability for a reaction to occur before evaporation is, then

$$p_{\rm r} = \sum_{\rm k=1}^{n_{\rm r}} p_k = 1 - (1-p_k)_{\rm r}^n \simeq n_{\rm r}p = \tau_{\rm ev}\theta_{\rm r}p_0\,, \quad (64)$$

if $p \ll 1$. The probability is independent of the migration timescale. It scales with the overall time an hydrogen atom stays on the grain surface. The treatment of surface reactions in the diffusion limit, i.e. the reactions are limited by the arrival timescales of species on the grain surfaces, by rate equations can lead to wrong results because an implicit assumption is that there is always more than one species on the surfaces or $N_{\rm s}\theta_i > 1$ with $\theta_i$ the surface coverage of species $i$. The dependence with respect to the activation barrier of the reaction is included in the factor $p$. A couple of gas-phase reactions

**Table 5.** Examples of grain surface reactions with activation barriers involving H atoms.

| Reactants | | Products | $E_{act}$ [K] |
|---|---|---|---|
| H + CO | $\longrightarrow$ | HCO | 1000 to 2500 |
| H + $O_2$ | $\longrightarrow$ | $HO_2$ | 1200 |
| H + $H_2O_2$ | $\longrightarrow$ | $H_2O$ + OH | 1400 |
| H + $O_3$ | $\longrightarrow$ | $O_2$ + OH | 450 |
| H + $C_2H_2$ | $\longrightarrow$ | $C_2H_3$ | 1250 |
| H + $C_2H_4$ | $\longrightarrow$ | $C_2H_5$ | 1100 |
| H + $H_2S$ | $\longrightarrow$ | SH + $H_2$ | 860 |
| H + $N_2H_2$ | $\longrightarrow$ | $N_2H$ + $H_2$ | 650 |
| H + $N_2H_4$ | $\longrightarrow$ | $N_2H_3$ + $H_2$ | 650 |

**Table 6.** Examples of radical-radical surface reactions.

| Reactants | | Products |
|---|---|---|
| H + O | $\longrightarrow$ | OH |
| H + OH | $\longrightarrow$ | $H_2O$ |
| H + C | $\longrightarrow$ | CH |
| H + CH | $\longrightarrow$ | $CH_2$ |
| H + $CH_2$ | $\longrightarrow$ | $CH_3$ |
| H + $CH_3$ | $\longrightarrow$ | $CH_4$ |
| H + N | $\longrightarrow$ | NH |

with activation barrier become possible on grain surfaces. A sample of surface reactions with their activation barrier (expressed in K) are listed in Table 5.

Another type of surface reactions describes the case that one of the coreactants is adsorbed on the grain surface while the second one arrives from the gas phase and collides with the adsorbed species. These reactions were proposed by Eley-Rideal (Fig. 10). Surface chemistry involves many assumptions in the rates and the treatment of the rates (rate equations or stochastic or Monte-Carlo simulations) as well in the rates themselves. Nevertheless its importance is paramount since many important molecules from molecular hydrogen to perhaps amino-acids via methanol are most likely efficiently formed on grain surfaces. Formation of molecular hydrogen on grain surfaces is an active field of research by itself. For example, Cazaux & Tielens (2004) developed a very comprehensive model for $H_2$ formation, where the Langmuir-Hinshelwood mechanism is considered for grain at temperatures below 100 K and the Eley-Rideal mechanism is considered for warm grains on which only chemisorbed atomic hydrogen can be present.

### 8.2 Example: Formation of water on grain surfaces

It is known since the work of Jones & Williams (1984) that the formation of a water ice mantle on dust grains requires surface reactions because gas-phase chemistry is not capable of synthesizing sufficient water molecules. This contrasts with another common solid species CO, which is believed to be accreted from the gas phase. Deuterium enrichment in water ice should therefore reflect the specificity of its formation and differ from enrichment of molecular species primarily formed in the

gas phase like $DCO^+$, HDCO, etc.. The formation of solid $H_2O$ proceeds via two exothermic reactions of Langmuir-Hinshelwood type. The first reaction is the formation of the hydroxyl radical OH from the addition of H to O. This reaction is fast ($\sigma = 5$ Å$^2$). The reaction of OH with H has two competing results: either H abstracts a hydrogen from OH and leaves the surface in the form of $H_2$, or a water molecule is synthesized. Since the former path is endothermic and has a large barrier, the latter highly exothermic path is favored in interstellar conditions. It should be noted that the formation of $H_2O$ releases enough energy for a significant fraction of water molecules to overcome the adsorption barrier and enrich the gas phase in water molecules. Most of the time, the grain surface acts as a heat sink, allowing the molecules to thermalize rapidly with the surface, therefore building up the icy mantle.

### 8.3 Grain charging and surface charge chemistry

Grains are predominantly negatively-charged in low-UV gas because the collision of a grain with an electron is much faster than the collision with a cation. The electron attachment rate onto a neutral grains is

$$k_{\rm e,n} = n_{\rm e} S_{\rm e} \sqrt{\frac{8kT_{\rm e}}{\pi m_{\rm e}}} \sigma_{\rm dust} \,, \tag{65}$$

where $T_{\rm e}$ is the electron temperature assumed equal to the gas kinetic temperature, $S_{\rm e}$ is the sticking coefficient for electron attachment, assumed to be 0.5, $\sigma_{\rm dust}$ is the geometrical cross-section of a grain of radius $a$, and $m_{\rm e}$ is the mass of an electron. For positively-charged grains ($Z_{\rm d} > 0$) the electron recombination rate is enhanced by Coulomb attraction

$$k_{\rm e,+} = k_{\rm e,n} \left(1 + \frac{W_{\rm c}}{kT}\right) , \tag{66}$$

where $W_{\rm c}$ is an extra work function that depends on the grain charge (Weingartner & Draine 2001). A simple extra work function is

$$W_{\rm c} = \frac{Z_{\rm d} e^2}{a} \,. \tag{67}$$

On the contrary, the recombination rate is lower if the grain is negatively charged ($Z_{\rm d} < 0$)

$$k_{\rm e,-} = k_{\rm e,n} \exp\left(\frac{W_{\rm c}}{kT}\right). \tag{68}$$

If a grain is positively charged, the Coulomb attraction between the grain and an electron effectively increases the photoelectric work function $W_{\rm eff} = W_0 + W_{\rm c}$. The recombination of positively charged ions and molecules have rates that are included explicitly. We consider that endothermic recombinations have energy barriers equal to the endothermicity of the reaction. The charge-exchange rates between a dust grain of charge $Z_{\rm d}$ and a cation can be derived from the rates with electrons.

Thermionic emission is the emission of an electron due to the transfer of momentum from an excited phonon to an electron. The rate follows from the Richardson-Dushman theory

$$k_{\rm RD} = \frac{4\pi m_e k^2}{h^3} T_d^2 \, \exp\left(\frac{W_{\rm eff}}{kT_d}\right) \sigma_{\rm dust} \,, \tag{69}$$

where $T_d$ is the dust temperature. The grain charge $Z_{\rm d}$ is determined by balancing the photoemission rate and the thermionic rate with the recombination rates.

An atomic hydrogen or molecular hydrogen impinging onto the grain can either transfer momentum or energy to the grain surface such that an electron is ejected (collisional electron detachment) with a rate

$$k_{\rm cd}^{\rm d} = \sigma_{\rm dust} \sqrt{\frac{8kT}{\pi m_{\rm n}}} \exp\left(-\frac{W_{\rm eff}}{kT}\right). \tag{70}$$

Gas-phase cations can recombine with a negatively-charged grain without dissociation because the excess energy is used to overcome the adsorption of the neutral species and the rest of the energy is transferred to surface phonons.

## 9 PAH chemistry

The exact reactions leading to the formation of Polycyclic Aromatic Hydrocarbons (PAHs) are not known. PAHs are most likely formed in the envelope of carbon-rich AGB stars and not in protoplanetary disks. The main process likely to lead to the formation of PAHs is the condensation of short carbon chains. Condensation is the name given to chemical processes leading to the formation of new C–C bondings in organic compounds. In the case of the formation of aromatic compounds, this process consists in the ion-molecule or in the radical-molecule addition of short unsaturated aliphatic molecules such as alcenes, allenes and alcynes.

On the other hand PAHs can be destroyed in disks. PAH destruction is governed by the loss of carbon fragments upon absorption of one or more UV photons. C–C bonds are a few eV stronger than C–H bonds, thus carbon is lost only from completely dehydrogenated PAHs. However, PAHs are extremely stable against UV photodissociation because PAHs can relax through cascades in their vibrational states. The probability of photodissociation can be expressed by the relation

$$p_d(E) = \frac{k(E)}{k(E) + k_{\rm IR}(E)}\,, \tag{71}$$

where $k(E)$ and $k_{\rm IR}(E)$ are respectively the rate coefficients for the dissociation and for the infrared radiative relaxation channels.

PAHs can become the main charge carriers in disks because of their abundances and electron affinity. In protoplanetary disks, their abundances are lower by a factor $f_{\rm PAH} = 10^{-1}$–$10^{-3}$ compared to their interstellar abundance of $3\times10^{-7}$. We can use the circumcoronene ($C_{54}H_{18}$) as typical PAHs that are large enough to escape photodissociation in disks around HerbigAe stars. The circumcoronene can be once negatively-charged ($PAH^-$) and three times positively charged by absorbing a UV with energy below 13.6 eV or by charge exchange reactions ($PAH^+$, $PAH^{2+}$, $PAH^{3+}$). PAHs are not formed or destroyed in many chemical networks and only exchange charges with other positively-charged species (for example $H^+$, $He^+$, $Mg^+$, $Fe^+$, $Si^+$, $S^+$, $HCO^+$). Chemical reaction rates involving PAHs are highly uncertain. Most of the rates are extrapolations from a few existing laboratory or theoretical rates and are discussed in the following sections.

### 9.1 Photoionization and photodetachment by stellar or interstellar photons

Stellar and interstellar ultraviolet photons ionize neutral and ionized PAHs in disk surfaces

$$\mathrm{PAH} + h\nu \rightarrow \mathrm{PAH}^+ + \mathrm{e}\,. \tag{72}$$

The photoionization rates at each disk location are computed by integrating the product of the photoionization cross-sections calculated using the PAH model of (Li & Draine 2001) with the internal

UV field obtained by solving the continuum dust radiative transfer and a yield computed according to the prescription of (Jochims et al. 1996). PAH self-shielding is taken into account. $PAH^-$ can loose its electron by absorbing a stellar or interstellar UV photon (photodetachment)

$$PAH^- + h\nu \rightarrow PAH + e^-. \tag{73}$$

The rates are computed the same way as for the photonionization.

### 9.2 Energetic particles induced photoionization and photodetachment

If $H_2$ is collisionally excited to Rydberg states by fast 'secondary' electrons generated by energetic particles (cosmic ray X-ray, or radioactive decay), the ionization of hydrogen fluoresce in the ultraviolet. The fluorescence photons have enough energies to ionize a PAH

$$PAH + MUV \rightarrow PAH^+ + e\,, \tag{74}$$

or detach an electron from a PAH anion

$$PAH^- + MUV \rightarrow PAH + e^-\,, \tag{75}$$

where MUV stands for UV generated by gas interaction with MeV particles. The number of fluorescence photons with energies between 7.1 and 14.6 eV is $f_{\rm Ryd}\zeta n_{\rm H}$, where $f_{\rm Ryd}$ is the fraction of the secondary electrons that excite the $H_2$, $\zeta$ is the total rate ($s^{-1}$) of hydrogen ionization (cosmic ray, X-ray, and radioactive decay). We adopt a value of 0.15 for $f_{\rm Ryd}$. The rate coefficient for photoionization triggered by energetic events is

$$k_{\rm pi,MeV} = 0.15\,\zeta\,n_{\rm H}\,g_{\rm PAH}\,y_{\rm pi}\ {\rm cm^{-3}\ s^{-1}}, \tag{76}$$

where $g_{\rm PAH}$ is the fraction of the photons absorbed by the neutral or positive PAHs compared to the total opacity and $y_{\rm pi}$ is the yield of photoionization. Likewise, the rate coefficient for photodetachment is

$$k_{\rm pd,CR} = 0.15\,\zeta\,n_{\rm H}\,g_{\rm PAH^-}\,y_{\rm pd}\ {\rm cm^{-3}\ s^{-1}}\,, \tag{77}$$

where $g_{\rm PAH^-}$ is the fraction of the photons absorbed by the negative PAHs and $y_{\rm pd}$ is the yield of photodetachment. Thes reactions may be important in the UV-shielded regions of disks.

### 9.3 Electron recombination

The electron recombination rates with singly-ionized PAHs

$$PAH^+ + e^- \rightarrow PAH \tag{78}$$

are calculated following a classical formalism by assuming that PAH-cations and electrons interact via a Coulomb potential

$$k_{\rm er} = 4.1\times10^{-5}\,\phi_{\rm PAH}\,f(a)\left(\frac{N_{\rm c}}{50}\right)^{1/2}\left(\frac{100\ {\rm K}}{T}\right)^{1/2}\ {\rm cm^3\ s^{-1}}, \tag{79}$$

where $N_{\rm c}$ is the number of carbon atoms and $\phi_{\rm PAH}$ a correction factor for the disk shape $\phi_{\rm PAH} = \sigma_{\rm disc}/\sigma_{\rm sphere}$ between 0.1 and 0.8 and $f(a)$ is a correction factor for small PAHs (explained

below). The recombination is essentially not dissociative for the large PAHs present in disks. For multiply-ionized PAHs, the recombination rate is enhanced

$$k'_{\rm er} = k_{\rm er} \times \left(1 + \frac{W_0}{kT_{\rm e}}\right), \tag{80}$$

where $W_0$ is calculated according to Weingartner & Draine (2001). For PAHs with less than 20 carbon atoms, an additional correction factor has to be applied to match the experimental data

$$f(a) = (1 - \exp(-12 \times a/l_{\rm e}))/(1.0 + \exp(12 - N_{\rm C})), \tag{81}$$

where $a$ is the PAH radius in cm and $l_{\rm e} = 10^{-7}$ cm. Alternatively, Flower & Pineau des Forêts (2003) a size-independent rate

$$k_{\rm er} = 3.3 \times 10^{-6} \left(\frac{300\ {\rm K}}{T}\right)^{1/2}\ {\rm cm}^3\ {\rm s}^{-1}. \tag{82}$$

Both rates can be reconciled if we take $\phi_{\rm PAH} \simeq 0.2$. For PAHs with 10 carbon atoms or less, the recombinations are dissociative.

### 9.4 Electron attachment

Electrons can attach on neutral PAHs. Experiments have shown that the electron attachment cross section is a strong function of the electron affinity, which changes the electron sticking coefficient $S_{\rm PAH}({\rm e})$. The electron attachment rates can be written as

$$k_{\rm ea} = S_{\rm PAH}({\rm e})\, k_{\rm f}\,, \tag{83}$$

where $k_{\rm f}$ is the electron capture rate. We adopt the sticking coefficient analytical formula

$$S_{\rm PAH}({\rm e}) = \frac{1 - {\rm e}^{-a/l_{\rm e}}}{1 + {\rm e}^{(20-N_{\rm c})}}\,, \tag{84}$$

where $a$ is the radius of the PAH in cm and $l_{\rm e}$ is the electron escape length equal to $10^{-7}$ cm. The capture rate follows a Langevin law and thus does not depend on the temperature

$$k_{\rm f} = 8.5 \times 10^{-7} \phi_{\rm PAH} \sqrt{N_{\rm c}}\,. \tag{85}$$

Large PAHs ($N_{\rm c} > 20$) have electron affinity large enough (∼1 eV) such that the electron sticking coefficient on PAHs, $S_{\rm PAH}({\rm e})$, is close to unity. The electron attachment rates are approximated by

$$k_{\rm ea} = 8.5 \times 10^{-7}\, S_{\rm PAH}({\rm e})\, \phi_{\rm PAH} \left(\frac{N_{\rm c}}{50}\right)^{1/2}\ {\rm cm}^3\ {\rm s}^{-1}\,. \tag{86}$$

The rates are high compared to atomic electronic attachment rate coefficients, whose values are $10^{-16} - 10^{-14}$ cm$^3$ s$^{-1}$. The formula is consistent with the measured value of $10^{-9}$ cm$^3$ s$^{-1}$ for anthracene ($C_{14}H_{10}$).

### 9.5 Mutual neutralization

The mutual neutralization reactions between any atomic cation $X^+$ and PAH

$$X^+ + PAH^- \rightarrow X^* - PAH \rightarrow X + PAH^* \tag{87}$$

proceeds at the rate

$$k_{\rm mn} = 2.9 \times 10^{-7} \phi_{\rm PAH} \left(\frac{12\ {\rm amu}}{m_{\rm X}}\right)^{1/2} \left(\frac{100\ {\rm K}}{T}\right)^{1/2} \left(\frac{N_{\rm c}}{50}\right)^{1/2}\ {\rm cm^3\ s^{-1}}\,, \tag{88}$$

where $m_{\rm X}$ is the mass of species X and amu is the value of the atomic mass units. For a molecular cation $AH^+$ the mutual neutralization can be dissociative

$$AH^+ + PAH^- \rightarrow AH^* - PAH \rightarrow A + H + PAH\,, \tag{89}$$

or not

$$AH^+ + PAH^- \rightarrow AH^* - PAH \rightarrow AH + PAH^*\,. \tag{90}$$

The branching ratio between the two modes is unknown. In the gas phase, electronic recombinations are dissociative because the ionization potentials are higher than the A-H bond energy. In the case of the recombination with negatively-charged PAHs the excess energy can be transferred to the PAHs. Here, both branches are assumed to have the same probability (0.5). Also, it is assumed that all atomic and molecular ions react with $PAH^-$.

### 9.6 Collisional detachment

Neutral species can detach the electron from negatively-charged PAHs

$$PAH^- + X \rightarrow PAH + X + e^-. \tag{91}$$

The rate follows the prescription of Flower & Pineau des Forêts (2003)

$$k_{\rm nd} = 1.5 \times 10^{-8}\, \phi_{\rm PAH} \left(\frac{1\ {\rm amu}}{m_{\rm X}}\right)^{1/2} \left(\frac{N_{\rm c}}{50}\right)^{1/2} {\rm e}^{-5500/T}\ {\rm cm^3\ s^{-1}}\,, \tag{92}$$

with $\phi_{\rm PAH} = 0.2$. The activation barrier is $E_{\rm a} = 5500$ K. Therefore, PAHs will be more neutralized by this process in hot disk midplanes.

### 9.7 Charge exchange reactions

Neutral and positively-charged PAHs can undergo charge exchanges with ions

$$X^+ + PAH^{n+} \rightarrow X + PAH^{(n+1)+}, \tag{93}$$

where $n \geq 0$. However, the Coulomb repulsion makes that for most gas temperatures, the rates for $n > 0$ are virtually zero. The criterium for the reaction to proceed is that the reaction is energetically allowed, i.e. the ionization potential (I.P.) of species X is higher than that of $PAH^{n+}$. Flower & Pineau des Forêts (2003) adopted a reaction probability of 0.1 per collision. We adopt the rate coefficients of the form

$$k_{\rm ce} = 2.9 \times 10^{-8}\, \phi_{\rm PAH} \left(\frac{1\ {\rm amu}}{m_{\rm X}}\right)^{1/2} \left(\frac{100\ {\rm K}}{T}\right)^{1/2} \left(\frac{N_{\rm c}}{50}\right)^{1/2}\ {\rm cm^3\ s^{-1}}\,. \tag{94}$$

Tielens (2010) also considers a double electron transfer from $He^+$ to neutral PAHs, because of the high value of the helium ioniation potential

$$He^+ + PAH \rightarrow He + PAH^{2+} + e\,, \tag{95}$$

with the rate

$$k_{\rm di} = 1.1 \times 10^{-8}\, \phi_{\rm PAH} \left(\frac{N_{\rm c}}{50}\right)^{1/2} \ {\rm cm^3\ s^{-1}}\,. \tag{96}$$

Inversely, positively-charged PAHs can gain an electron from ions

$$X + PAH^{n+} \rightarrow X^+ + PAH^{(n-1)+}\,. \tag{97}$$

Among the major atomic and molecular species, only sodium (Na) has an I.P. that is lower than that of the adopted PAH.

### 9.8 PAH adsorption and desorption

In addition PAHs can adsorb onto grain surfaces whether they are coated with water ice or not. In the absence of measured rates for all the PAHs, we assume a linear dependance of the desorption energy with the number of carbon and hydrogen atoms of the PAH based on the method of fragment constant. The linear behavior is consistent with the additivity of van der Waals interactions. Desorption energies $E_{\rm des}$ measured in the laboratory vary from $E_{\rm des} \simeq 5600$ K for benzene $C_2H_6$ up to $E_{\rm des} \simeq 18900$ K for pentacenene $C_{22}H_{14}$. It should be noted that the surface on which the PAHs are adsorbed varies. The adopted law is

$$E_{\rm des} = (482 \times N_{\rm C}) + (464 \times N_{\rm H})\ {\rm K}, \tag{98}$$

where $E_{\rm CC} = 482$ K is the fitted desorption energy per graphene-like carbon, and $E_{\rm CH} = 946$ K is the fitted energy per benzene-like carbon and its adjoining H-atom. Graphene-like carbons are C-atoms with three covalent bonds with carbons, whereas benzene-like carbon have two covalent bonds with carbons and one bond with a hydrogen atom. Graphenes are PAHs where all the hydrogens have been stripped away (dehydrogenated). The desorption energies are consistent with the theoretical values of Mészár et al. (2013). Theoretical and experimentally measured value for $E_{\rm CC}$ vary from 464 to 928 K in the literature (Thrower et al. 2009). The fitting formula is valid for PAHs made of up to 100 carbon atoms. For bigger PAHs, the formula gives values that are larger than that of graphite ($E_{\rm des} = 86240$ K). For circumcoronene, the estimated desorption energy is 34380 K. In disks, PAHs should stick onto silicate grains and to each other. The desorption of PAHs occurs thermally, induced by cosmic ray hits on the grains, and by absorption of UV photons.

Adsorbed PAHs are easily charged upon UV irradiation. However, electrons on the grains will rapidly recombine with the PAH cations. Therefore we assume that there is no PAH charging on surfaces. The interaction between a negatively-charged grain and a negative PAH is repulsive and assumed not to occur. In the disk regions where both the PAHs and the grains are negatively charged, PAHs cannot adsorb onto grains.

**Acknowledgements** The research leading to these results has received funding from the European Union Seventh Framework Programme FP7-2011 under grant agreement no 284405.

## References

Agúndez, M., Goicoechea, J. R., Cernicharo, J., Faure, A., & Roueff, E. 2010, ApJ, 713, 662

Bass, L., Su, T., Chesnavich, W., & Bowers, M. 1975, Chemical Physics Letters, 34, 119

Burke, J. R. & Hollenbach, D. J. 1983, ApJ, 265, 223

Cazaux, S. & Tielens, A. G. G. M. 2004, ApJ, 604, 222

Chaabouni, H., Bergeron, H., Baouche, S., et al. 2012, A&A, 538, A128

Chyba, C. & Sagan, C. 1992, Nature, 355, 125

Dyson, J. E. & Williams, D. A. 1997, The physics of the interstellar medium

Ehrenfreund, P. & Charnley, S. B. 2000, ARA&A, 38, 427

Flower, D. R. & Pineau des Forêts, G. 2003, MNRAS, 343, 390

Garrod, R. T. & Pauly, T. 2011, ApJ, 735, 15

Garrod, R. T., Wakelam, V., & Herbst, E. 2007, A&A, 467, 1103

Hasegawa, T. I., Herbst, E., & Leung, C. M. 1992, ApJS, 82, 167

Helling, C., Woitke, P., Rimmer, P. B., et al. 2014, Life, 4, 142

Hollenbach, D. & McKee, C. F. 1979, ApJS, 41, 555

Hollenbach, D. & Salpeter, E. E. 1970, J. Chem. Phys., 53, 79

Hugo, E., Asvany, O., & Schlemmer, S. 2009, J. Chem. Phys., 130, 164302

Jochims, H. W., Baumgaertel, H., & Leach, S. 1996, A&A, 314, 1003

Jones, A. P. & Williams, D. A. 1984, MNRAS, 209, 955

Klippenstein, S. J., Yang, Y.-C., Ryzhov, V., & Dunbar, R. C. 1996, J. Chem. Phys., 104, 4502

Lequeux, J. 2005, The Interstellar Medium

Li, A. & Draine, B. T. 2001, ApJ, 554, 778

Mészár, Z. E., Hantal, G., Picaud, S., & Jedlovszky, P. 2013, The Journal of Physical Chemistry C, 117, 6719

Öberg, K. I., Murray-Clay, R., & Bergin, E. A. 2011, ApJL, 743, L16

Smith, I. W. M. 2008, Chem. Soc. Rev., 37, 812

Thrower, J. D., Collings, M. P., Rutten, F. J. M., & McCoustra, M. R. S. 2009, J. Chem. Phys., 131, 244711

Tielens, A. G. G. M. 2010, The Physics and Chemistry of the Interstellar Medium

van Dishoeck, E. F., Jonkheid, B., & van Hemert, M. C. 2006, Faraday Discussions, 133, 231

Veeraghattam, V. K., Manrodt, K., Lewis, S. P., & Stancil, P. C. 2014, ApJ, 790, 4

Weingartner, J. C. & Draine, B. T. 2001, ApJS, 134, 263